Review | Open Access

Energy Materials

Wang *et al. Energy Mater.* **2026**, *6*, 600064 **DOI:**10.20517/energymater.2026.36

The effect of additive engineering and machine learning on high performance perovskite solar cells

Han Wang, Jiazhi Meng, Feiyu Kang, Guodan Wei*

Keywords:
Perovskite solar cells, additive engineering, machine learning, defect passivation, data-driven discovery

Citation: Wang, H.; Meng, J.; Kang, F.; Wei, G. The effect of additive engineering and machine learning on high performance perovskite solar cells. *Energy Mater.* **2026**, *6*, 600064. https://dx.doi.org/10.20517/energymater.2026.36

Received: 18 Mar 2026 **First Decision:** 16 Apr 2026 **Revised:** 29 Apr 2026 **Accepted:** 25 May 2026 **Published:** 17 Jun 2026

Academic Editor: Soo Young Kim
Copy Editor: Fangling Lan
Production Editor: Fangling Lan

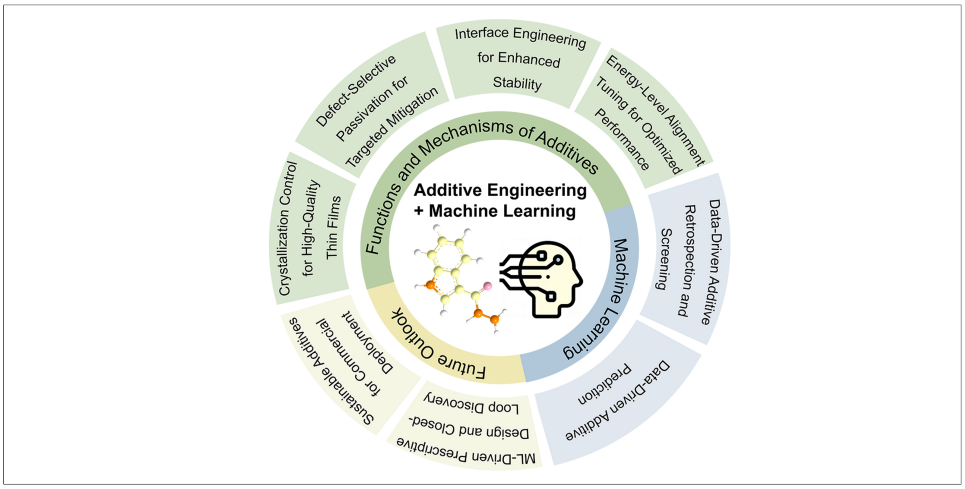

Abstract

Additive engineering has emerged as a powerful strategy for enhancing the efficiency and stability of perovskite solar cells (PSCs), enabling precise control over crystallization kinetics, defect passivation, interfacial energetics, and long-term environmental stability. By controlling nucleation and crystal growth, and thereby optimizing film morphology, additives effectively suppress non-radiative recombination and ion migration, addressing key challenges in the path toward commercialization. However, the conventional discovery process remains largely empirical and time-consuming. The integration of machine learning (ML) offers a promising avenue for data-driven screening, rational molecular design, and accelerated optimization of additive systems. ML models trained on experimental datasets and augmented with density functional theory and molecular dynamics simulations can predict interactions between additives and perovskites, identify performance-determining descriptors, and guide the discovery of novel functional molecules. This review systematically outlines the multifaceted roles of additives in PSCs, from crystallization regulation to interfacial stabilization. We further highlight the synergy between ML and additive engineering, emphasizing its potential to establish a predictive, intelligent framework for next-generation photovoltaic materials.

Institute of Materials Science, Tsinghua Shenzhen International Graduate School, Tsinghua University, Shenzhen 518000, Guangdong, China.

***Correspondence to:** Prof. Guodan Wei, Institute of Materials Science, Tsinghua Shenzhen International Graduate School, Tsinghua University, Shenzhen 518000, Guangdong, China. E-mail: weiguodan@sz.tsinghua.edu.cn

INTRODUCTION

Over the past decade, metal halide perovskite solar cells (PSCs) have emerged as a leading candidate for next-generation photovoltaic technologies, driven by their exceptional optoelectronic properties[1,2], including strong light absorption[3,4], long carrier diffusion lengths[5,6], tunable direct bandgaps[7,8], and intrinsic defect tolerance[9,10], as well as compatibility with low-cost[11,12], solution-based fabrication[13,14]. Since their initial demonstration in 2009 with a power conversion efficiency (PCE) of just 3.8%[15], single-junction PSCs have rapidly advanced, achieving certified efficiencies of over 27.0%[16], which now rival those of commercial crystalline silicon solar cells. Despite these advances, operational instability arising from environmental stressors such as heat[17,18], moisture[19,20], light[21,22], and electrical bias[23], as well as ion migration[4,24] and defect accumulation[25] in polycrystalline films, continues to limit the long-term stability and durability of PSCs. Furthermore, scaling from laboratory-scale devices to large-area modules introduces significant hurdles in achieving uniform, reproducible, and stable perovskite films, posing considerable challenges to both device performance and widespread commercialization[26,27].

To overcome these limitations, additive engineering has become one of the most versatile and effective strategies. By incorporating trace amounts of functional molecules into perovskite precursor solutions or interfacial layers, researchers have achieved substantial improvements in film morphology[28,29], defect passivation[10,30], energy-level alignment[31,32], and long-term stability[33,34]. Additives serve multiple critical functions, including modulation of crystallization kinetics to promote the formation of large-grain, pinhole-free films[35,36], passivation of undercoordinated ions and vacancies to suppress non-radiative recombination and ion migration[37,38], and optimization of interfacial energetics to enhance charge extraction while providing protective barriers against environmental degradation[39,40]. Collectively, these multifunctional effects establish additive engineering as a pivotal approach in advancing PSC performance and stability. However, conventional trial-and-error strategies are inherently inefficient in navigating the immense chemical space and deciphering the intricate interplay between additives, perovskite chemistry, and device architecture. The vast chemical diversity of potential additives and their complex, often interdependent interactions with perovskite systems pose significant challenges for rational design, thereby necessitating the integration of advanced computational and data-driven methodologies. In this regard, machine learning (ML) is emerging as a transformative tool for accelerating additive discovery and optimization. ML models trained on experimental datasets and high-throughput simulations, using molecular descriptors as input features, can rapidly identify promising candidates, predict their impact on crystallization dynamics, defect passivation, and interfacial stability, and propose novel molecular scaffolds that are difficult to identify through conventional approaches[41]. These synergistic advances highlight the potential of merging additive engineering with ML to establish predictive design frameworks, ultimately enabling the development of high-performance, stable, and scalable perovskite photovoltaics.

Although extensive research has demonstrated the functional versatility of diverse additives in perovskite systems, the absence of unified design principles and the trial-and-error nature of additive discovery continue to hinder rational device optimization. At the same time, the advent of ML and multiscale simulations provides powerful tools to accelerate the exploration of the vast chemical space of potential additives, offering significant opportunities to establish predictive frameworks for additive design. Given these opportunities and challenges, a systematic understanding of additive engineering in PSCs is both timely and necessary. In this review, we provide a comprehensive overview and categorization of functional additives, analyze their working mechanisms within the bulk and across interfaces, and highlight the integration of ML with multiscale simulations to enable predictive materials design in perovskite photovoltaics. By bridging mechanistic insights with data-driven approaches, this work aims to outline the state-of-the-art strategies, identify key challenges, and propose future directions for advancing PSCs toward high efficiency, stability, and scalability.

FUNCTIONS AND MECHANISMS OF ADDITIVES

Crystallization control for high-quality thin films

The formation of high-quality perovskite films is governed by a series of additive-driven interventions across multiple stages, ranging from ordering colloidal distribution and tailoring intermediate phase selection to controlling grain coarsening and nucleation. Each of these modulations is strategically engineered to eliminate defects and optimize device performance.

Ordering colloidal distribution and stacking

At the earliest stage, perovskite inks are best understood as colloidal suspensions rather than ideal molecular solutions. Their stability is primarily governed by the balance between electrostatic repulsion and van der Waals attraction, which determines whether solute species remain dispersed or undergo uncontrolled aggregation[42]. Additives serve as colloidal stabilizers during this stage by suppressing spontaneous clustering and homogenizing the level of supersaturation. A cornerstone strategy in this regulatory paradigm involves the incorporation of tin(II) fluoride (SnF_2), in which fluoride ions selectively coordinate with Sn^{2+} species to mitigate oxidation-induced structural disorders and stabilize Sn-Pb inks[43]. However, a critical mechanistic trade-off underpins this canonical approach. While moderate SnF_2 levels effectively passivate surface Sn(IV)-associated deep traps and extend carrier lifetimes, stoichiometric excesses paradoxically induce the stabilization of tin interstitial (Sn_i) defects. These Sn_i traps function as deleterious deep-level electronic states that introduce non-radiative recombination pathways, thereby necessitating a delicate equilibrium in defect management[44]. To circumvent these limitations, diverse alternative strategies have been developed to supplement or replace SnF_2. One direct approach is the use of sacrificial metallic Sn(0) powder, which reduces Sn^{4+} back to Sn^{2+} without introducing foreign ionic impurities[45]. A more versatile paradigm relies on multifunctional organic additives such as melamine, gallic acid, or theophylline, which provide sustained oxidative inhibition through robust C=N or C=O coordination[46,47]. In particular, melamine, acting as a highly symmetric Lewis base, has been shown to strongly coordinate with Sn^{2+} ions, effectively regulating the formation of iodostannate clusters and significantly enlarging colloidal dimensions. This molecular interaction is instrumental in navigating a second fundamental trade-off that requires balancing the intrinsically rapid nucleation typical of tin-halide perovskites with the necessity for sustained crystal growth. By retarding crystallization kinetics and simultaneously inhibiting Sn^{2+} oxidation, the melamine-coordinated system facilitates a more orderly crystal assembly. This synergistic effect minimizes defect-induced voltage loss and enhances the overall PCE[48]. The principle of colloidal and kinetic modulation further extends to other advanced organic framework additives. For example, small-molecule deformable additives can reshape the size distribution of colloids to decelerate crystallization while concurrently passivating defects to suppress stress accumulation[49]. In a similar vein, spatially isomeric fulleropyrrolidine derivatives illustrate how tailoring the steric structure of additives can enlarge colloidal aggregates and optimize crystallization kinetics, ultimately yielding highly uniform tin-based perovskites with low defect densities[50] [Figure 1A].

Tailoring intermediate phase selection

Once the colloidal framework is stabilized, additives intervene in the nucleation and intermediate-phase formation stage, where coordination chemistry and weak-anion interactions govern the transition from solvation complexes to crystalline nuclei. The incorporation of weakly coordinating anions such as chloride and thiocyanate facilitates the development of reversible halide-rich intermediates including $HPbI_{3-x}Cl_x$, which serve to homogenize nucleation and promote secondary recrystallization[51,52]. To precisely govern these processes, a fast-solidification and slow-growth strategy can be employed using a volatile acetonitrile solvent system in combination with non-volatile additives such as ammonium thiocyanate and methylammonium chloride[51]. The rapid evaporation of acetonitrile effectively freezes a uniform distribution of nuclei during the initial solidification phase[53]. Subsequently, the remaining high-boiling-point additives

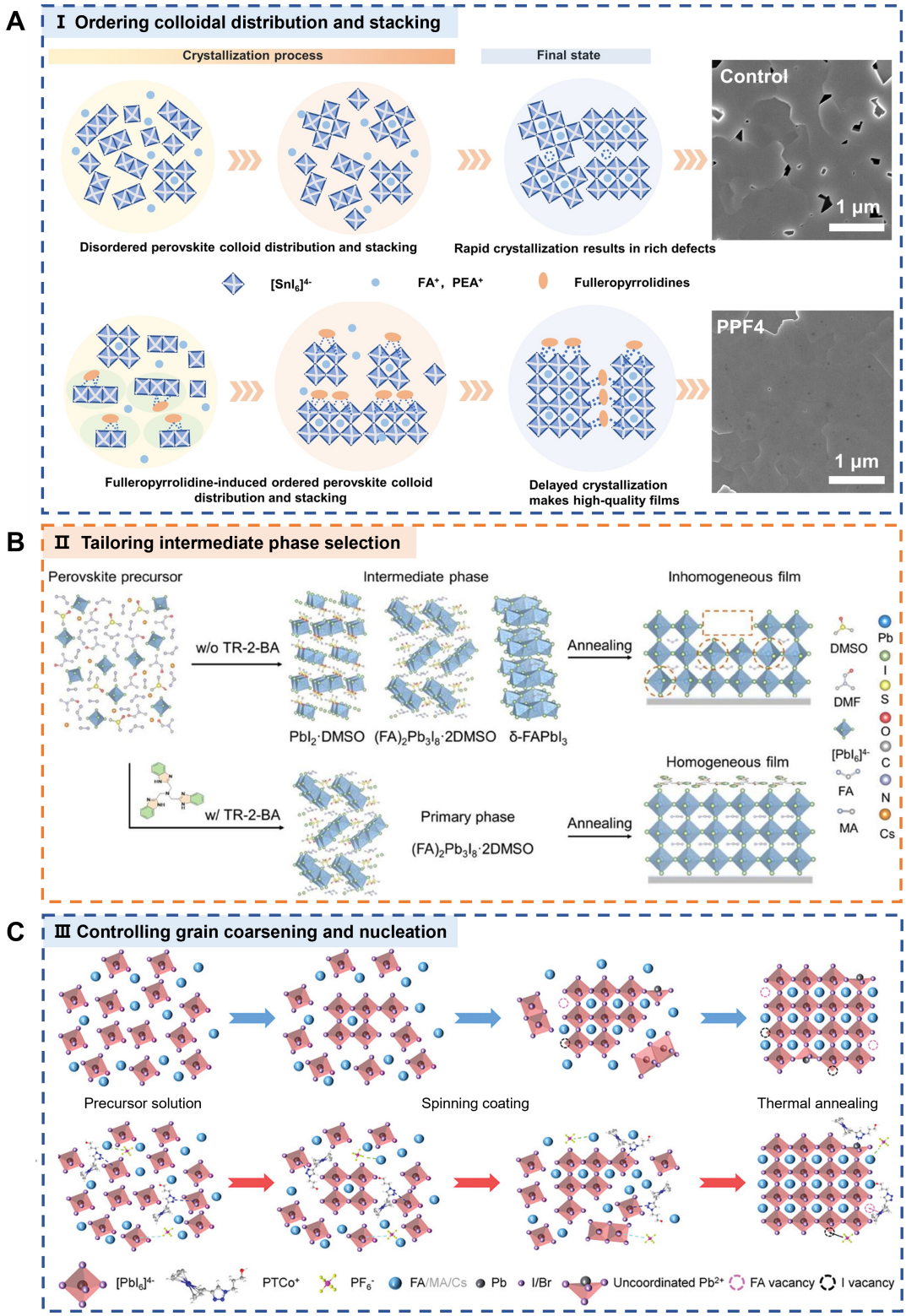

Figure 1. Additive-mediated regulatory mechanisms across the entire perovskite crystallization process. (A) Ordering colloidal distribution and stacking: Stacking configurations of perovskite colloids without (w/o) and with (w) fulleropyrrolidine. Reprinted with permission[50]. Copyright 2025, John Wiley and Sons. (B) Tailoring intermediate phase selection: Structural evolution of FA-based perovskites under additive-free and TR-2-BA-modified conditions. Reprinted with permission[57]. Copyright 2025, John Wiley and Sons. (C) Controlling grain coarsening and nucleation: Crystallization pathways without (w/o) and with (w) $PTCoPF_6$. Reprinted with permission[58]. Copyright 2024, John Wiley and Sons.

enable a controlled ripening process that allows the perovskite layer to achieve high crystallinity and superior morphological uniformity. Building on this foundation, strong Lewis-base donors such as dimethyl sulfoxide (DMSO) and N-methyl-2-pyrrolidone (NMP) stabilize coordination complexes and intermediate phases by forming stable PbI_2·solvent adducts, which delay the α-phase transition and extend the solvent-release window, thereby facilitating controlled crystallization and enhanced film quality[54,55]. This mechanism of intermediate regulation is vividly demonstrated in slot-die-coated $MAPbI_3$ inks processed with 2-methoxy-ethanol (2-ME). Within this system, a fundamental trade-off exists because the concentration of DMSO must be precisely tuned to govern the competition among different solvated species. An optimal amount of DMSO facilitates the formation of beneficial PbI_2·DMSO or solvated iodoplumbate intermediates that effectively suppress the emergence of undesirable $MAPbI_3$-2-ME crystalline phases[56]. Insufficient DMSO allows the formation of these deleterious solvated adducts that lead to high film porosity, whereas an excessive concentration can result in the retention of overly stable complexes that hinder efficient conversion into the perovskite lattice. Because these solvent-solute interactions directly dictate the kinetics of film drying and the subsequent crystallization pathway, they have profound consequences for the final grain size and the optoelectronic quality of the semiconductor layer. More sophisticated molecular additives offer a precise route to overcome the inherent sensitivity of solvent-solute equilibria during film formation. Specifically, the introduction of tris(2-benzimidazolylmethyl)amine (TR-2-BA) exemplifies how tailored intermolecular interactions can steer the coordination environment of precursor inks[57]. Through the formation of extensive hydrogen-bonding and coordination networks with DMSO, TR-2-BA effectively suppresses the stochastic formation of diverse solvated intermediates. This regulatory mechanism enforces the emergence of a singular and uniform $(FA)_2$·Pb_3I_8·2DMSO intermediate phase that bypasses the stringent requirements of DMSO stoichiometry previously discussed. Consequently, the homogenization of the intermediate phase ensures highly consistent nucleation and growth behaviors across varying fabrication conditions, leading to enhanced film reproducibility and significantly reduced defect densities in the resulting devices [Figure 1B].

Controlling grain coarsening and nucleation

Once a uniform and properly defined nucleation landscape is established, the subsequent phase of controlled crystal growth can proceed as a natural consequence. To guarantee that this progression translates into a high-quality thin film, additives must continue to function as kinetic regulators that prevent uncontrolled grain coarsening and sporadic secondary nucleation. Without such regulation during the growth phase, the expanding lattice remains susceptible to accumulating stress and forming non-radiative recombination centers at grain boundaries. Feng *et al.*[2] provided a compelling demonstration of this guided growth paradigm by introducing 4,4′-oxydibenzenesulfonyl chloride (OBSC), a bifunctional additive featuring two sulfonyl chloride groups on a flexible backbone. The unique spatial configuration of OBSC enables multisite coordination by strongly binding to undercoordinated Pb^{2+} through Pb-O interactions while simultaneously engaging formamidinium cations via hydrogen bonding. During the critical crystal growth phase, these robust intermolecular interactions stabilize the perovskite and solvent intermediate phases to precisely regulate the crystallization kinetics. This targeted molecular intervention effectively decelerates and homogenizes the overall grain growth process, thereby passivating high-energy surface domains and suppressing non-radiative recombination pathways. In a similar vein, the application of organometallic compounds further exemplifies how targeted structural design can sustain this orderly growth trajectory. Specifically, the introduction of 1-propanol-2-(1,2,3-triazol-4-yl) cobaltocenium hexafluorophosphate ($PTCoPF_6$) demonstrates a synergistic modulation of both kinetic control and comprehensive defect passivation[58]. The triazole ring within this organometallic salt coordinates strongly with undercoordinated lead to mitigate deep-level defects, while its cobaltocenium cations and hexafluorophosphate anions work concurrently to stabilize the overall lead-iodide framework and repair shallow-level vacancies. These robust chemical interactions systematically retard the crystallization rate to ensure that the previously established uniform nucleation landscape evolves naturally into steady grain coarsening. By sustaining this controlled

growth phase, $PTCoPF_6$ actively suppresses secondary nucleation events and enhances overall crystallinity [Figure 1C]. Ultimately, this seamless transition from uniform nucleation to carefully regulated crystal growth minimizes structural defects across all energy levels and establishes a robust foundation for superior device performance.

Collectively, the deployment of molecular additives transforms perovskite crystallization from a stochastic process into a precisely programmable pathway. This comprehensive regulatory paradigm systematically orchestrates three interdependent stages comprising colloidal stabilization, intermediate phase engineering, and kinetic growth control. Navigating these stages requires a careful reconciliation of inherent mechanistic trade-offs to ensure that suppressing one defect pathway does not inadvertently induce another. By successfully balancing these competing kinetic and thermodynamic demands, researchers can produce highly crystalline and defect-lean films necessary for scalable device fabrication. Moving forward, the evolution of additive engineering will increasingly rely on the rational design of multisite molecules. Compounds equipped with diverse coordinating groups possess the unique capability to govern the entire crystallization sequence from precursor homogenization to grain boundary passivation. To accelerate the discovery of such molecules, the integration of ML and high-throughput computational screening will be essential. These data-driven algorithms offer a powerful approach to explore vast chemical spaces and predict novel candidates that optimally satisfy the complex trade-offs across all three crystallization phases. Ultimately, coupling predictive computational models with targeted multisite additive synthesis will establish a robust foundation for the commercialization of highly efficient and reproducible perovskite optoelectronics.

Defect-selective passivation for targeted mitigation

In an ideal perovskite crystal, each constituent ion occupies its thermodynamically stable lattice site. However, in practice, the rapid crystallization kinetics of perovskite thin films, typically accompanied by post-deposition annealing, often lead to non-equilibrium conditions that inevitably result in the formation of diverse structural defects[59]. As illustrated in Figure 2, in polycrystalline films, these defects are typically categorized into point defects[60,61], surface, grain boundary, and interface defects[62-64], and extended defects such as secondary phases[65,66]. Each defect class introduces distinct electronic trap states that impair carrier dynamics by promoting non-radiative recombination, reducing carrier lifetimes, and limiting charge transport. Additive engineering has thus emerged as a highly versatile strategy for selectively passivating these diverse defect types across multiple length scales. A deep understanding of these defect-passivation mechanisms not only enables performance enhancement but also lays the essential groundwork for the integration of data-driven approaches, such as machine learning, in the rational design of next-generation perovskite optoelectronic materials.

Point defects

Among the most fundamental are point defects, which originate from atomic-scale deviations in stoichiometry or coordination and serve as primary sources of deep-level trap states. Point defects in halide perovskites, including anion vacancies (V_I, V_{Br})[67-69], cation vacancies (V_{MA}, V_{FA}, V_{Cs})[70-72], and antisite defects (e.g., I_{Pb}, Pb_I)[73-75], introduce deep-level trap states that accelerate Shockley-Read-Hall (SRH) recombination and thereby restrict device efficiency. Additive engineering has become a widely adopted strategy to mitigate these localized states.

Anion vacancies

The formation of anion vacancies directly leads to undercoordination of neighboring Pb^{2+} ions, rendering them electron traps via dangling bonds. Notably, the extensive research on additive molecules targeting undercoordinated Pb^{2+} has necessitated a dedicated summary in this review, as the emergence of anion

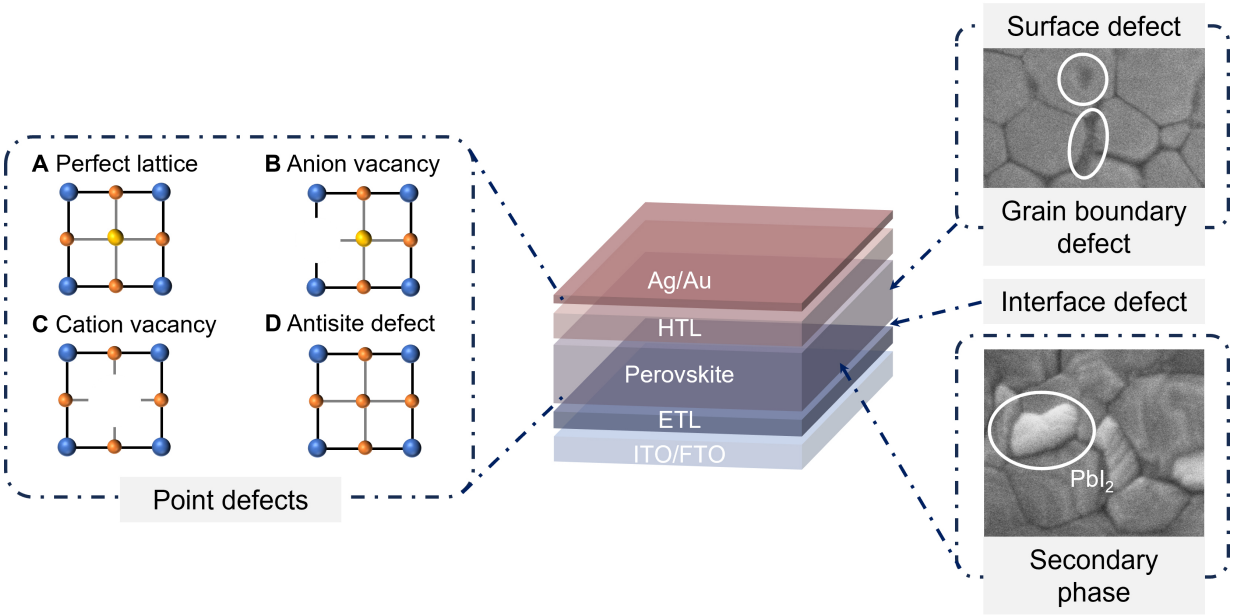

Figure 2. Schematic illustration of typical defects in perovskite materials and devices.

vacancies inevitably induces undercoordination, establishing an inherent correlation between these two interdependent defects[76-78]. For anion vacancies during perovskite film formation, halide additives such as methylammonium chloride (MACl) or lead chloride ($PbCl_2$) can transiently introduce Cl^- into intermediate phases or early-stage lattices, which are gradually released upon annealing[79,80]. This temporary incorporation suppresses the formation of anion vacancies and coordinates with undercoordinated lead centers, thereby reducing trap density and improving film quality. This strategy prolongs carrier lifetimes and enhances the photoluminescence quantum yield (PLQY), as confirmed by time-resolved photoluminescence (TRPL) measurements. However, the single use of MACl is often insufficient to suppress detrimental intermediate phases in precursor solutions. The methylammonium cation (MA^+) in MACl can undergo deprotonation to form methylamine, which subsequently reacts with the formamidinium cation (FA^+) to generate undesired species and lead to compositional heterogeneity at grain boundaries[81]. This complex degradation cascade and its associated solvent-driven oxidation reactions are illustrated in Figure 3. To counteract this vulnerability, Ma *et al.*[82] introduced 2-thiouracil (Th) as a multifunctional precursor stabilizer that provides targeted protection against methylammonium degradation. Because its acidity constant is lower than that of the methylammonium cation, this additive acts as a more effective proton donor to preferentially inhibit the initial deprotonation step. By halting the deprotonation process, it successfully arrests the subsequent chain of detrimental condensation and oxidation side reactions at their source. This strategic intervention maintains the precise stoichiometry of the precursor solution and enables the reproducible fabrication of high-quality PSCs even after a prolonged solution aging period of 30 days. Furthermore, excessive MACl concentrations can volatilize during annealing, resulting in void formation and morphological defects that act as shunting pathways, which may compromise long-term device stability. These structural limitations can be effectively mitigated by employing synergistic additives such as Lewis basic ionic liquids (e.g., 1,3-bis(cyanomethyl)imidazolium chloride ([Bcmim]Cl)) to stabilize the precursor chemistry, suppress unwanted intermediates, and simultaneously passivate anion vacancies and undercoordinated metal centers[1].

Undercoordinated Pb^{2+} is fundamentally defined as lead cations within the perovskite lattice that lack a complete surrounding sphere of halide ligands. This specific defect state exhibits an intrinsic correlation with

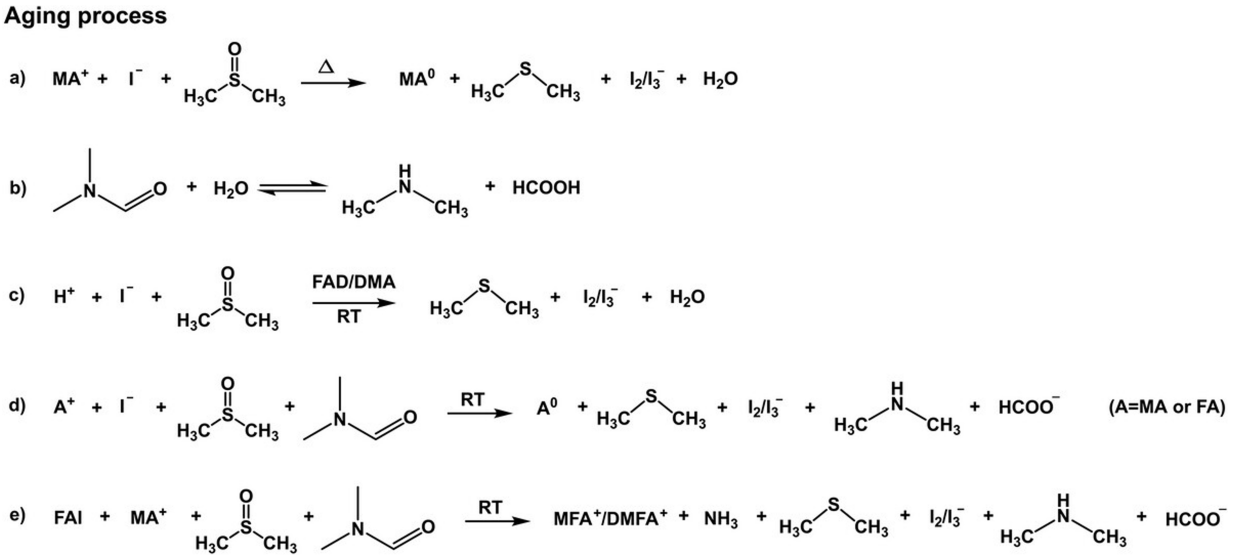

Figure 3. Degradation pathways in perovskite precursors. Reprinted with permission[81]. Copyright 2025, John Wiley and Sons.

anion vacancies. During crystallization and subsequent thermal annealing, the inevitable loss or volatilization of halide ions at grain boundaries and film surfaces generates vacant anionic sites[83]. The physical absence of these halides simultaneously strips the adjacent lead ions of their coordinating bonds and exposes them as unsaturated Pb^{2+} centers. Consequently, these exposed metal sites function as detrimental deep-level electron traps within the semiconductor bandgap, severely exacerbating non-radiative recombination pathways and thereby imposing a rigid limitation on the open-circuit voltage (V_{OC}) of the photovoltaic devices. One common approach is the use of Lewis-base molecules such as amines[84-86], carbonyls[87-89], thiols[90-92], and phosphates[93-95], which form strong coordination bonds with undercoordinated Pb^{2+} ions. For instance, Xie *et al*.[96] demonstrated that phosphoric acid derivatives (e.g., 3-phosphonopropionic acid (H3pp)) passivate undercoordinated Pb^{2+} via O-Pb interactions, stabilizing the film and suppressing ion migration. Another effective strategy involves multifunctional molecules such as urea, biuret, and thiourea derivatives. Liu *et al*.[97] demonstrated that amidinethiourea (ATU) effectively passivates undercoordinated Pb^{2+} via a targeted coordination mechanism in which the sulfur atom of the thiourea group donates lone-pair electrons to the empty orbitals of exposed metal centers to form robust coordination bonds. This strong chemical interaction successfully neutralizes the detrimental deep-level trap states associated with undercoordinated lead species, leading to significantly improved crystallinity, reduced defect density, and enhanced carrier mobility across the perovskite film. A third approach employs polydentate chelating agents such as 2-deoxy-2,2-difluoro-D-erythro-pentafuranous-1-ulose-3,5-dibenzoate (DDPUD) to implement a molecular locking strategy[74]. Distinct from conventional multisite additives that offer flexible or transient surface coordination, this locking paradigm leverages abundant electronegative functionalities including carbonyl and carbon-fluorine bonds to establish a rigid chelating network with undercoordinated Pb^{2+}. This firm chemical anchoring physically locks the perovskite surface lattice to relieve residual tensile strain, a critical mechanical stabilization that standard additives often fail to achieve. By securing the crystal surface and grain boundaries, the DDPUD molecule not only passivates interfacial defects but also establishes a robust barrier against environmental moisture, directly improving charge transport and long-term device stability.

Cation vacancies

While mitigating undercoordinated lead sites addresses a primary source of deep traps, the overall structural integrity of the perovskite lattice remains highly susceptible to the concurrent loss of A-site cations. This

vulnerability is fundamentally rooted in a thermodynamic coupling effect. Qu *et al.*[72] established that adjacent anion and cation vacancies exhibit a mutual promotion mechanism in which the presence of one defect significantly lowers the formation energy of the other. This intricate thermodynamic relationship dictates that functional additives must achieve synergistic defect passivation rather than targeting single defects. Cation vacancies severely disrupt the local charge balance and generate detrimental deep trap states. Building upon the molecular locking concept previously introduced for lead passivation, researchers have developed analogous synergistic systems to heal these cation vacancies. A representative example is the all-organic molecular lock fluorinated anilinium benzylphosphonate (FABP), which consists of a fluorophenylammonium cation and a fluorobenzyl phosphonate anion. The cation selectively occupies vacant formamidinium or methylammonium sites while the anion simultaneously compensates for missing halides. This dual action dramatically reduces trap density, suppresses non-radiative recombination, and extends carrier lifetimes from approximately 4 ns to beyond the detection limit, accompanied by a significantly improved PLQY[70]. Following this synergistic principle, N-methylammonium formate (NMACOOH) provides NMA^+ to fill cation vacancies while its $HCOO^-$ coordinates with Pb^{2+} to effectively suppress non-radiative charge losses[71]. In all-inorganic $CsPbI_3$ systems, alkylammonium bromides such as *N*,*N*,*N*-trimethyl-1-dodecanaminium bromide (DTABr) can heal Cs^+ vacancies through the strong coupling of their organic cations with the $[PbI_6]^{4-}$ octahedra. Concurrently, the Br^- ions passivate lead-related defects to yield enhanced photoluminescence (PL) intensity and prolonged carrier lifetimes[98]. For multifunctional small molecules, 2-hydrazinylpyrazine (2-HZP) exemplifies this dual-site mechanism through extensive hydrogen-bonding networks that increase the formation energy of FA-related vacancies while simultaneously coordinating with undercoordinated Pb^{2+}[72]. Furthermore, polymeric additives demonstrate superior multifunctional defect passivation capabilities, as exemplified by polyvinylpyrrolidone (PVP), which simultaneously passivates both cation and anion vacancies through the coordinated interactions of its amide group oxygen and nitrogen atoms. This comprehensive passivation mechanism effectively suppresses anion exchange reactions and photoinduced halide segregation to enhance both the crystalline integrity and the photovoltaic performance of the devices[99].

Antisite defects

Beyond the thermodynamic instability associated with ion vacancies, the perovskite lattice is equally vulnerable to the misplacement of its constituent elements. Antisite defects arise when ions occupy incorrect positions within the ABX_3 framework, commonly manifesting as iodine on a lead site (I_{Pb}) or lead on an iodine site (Pb_I). Because these misplaced species induce profound local charge imbalances and spatial distortions, they readily generate detrimental deep-level trapping centers that degrade device performance. To overcome these challenges, a widely adopted approach involves the introduction of tailored halide or pseudohalide anions that can integrate into the lattice framework to heal these defects. Cheng *et al.*[100] demonstrated that BF_4^- from potassium borofluoride (KBF_4) interacts with I_{Pb} to transform deep defect levels into shallow states, significantly reducing trap density. Likewise, Zhu *et al.*[101] introduced the ionic liquid 1-ethyl-3-methylimidazolium chloride (EMImCl) to show that Cl^- exhibits exceptionally low adsorption energy (0.46 eV) on the (110) crystal plane, enabling incorporation into the superficial lattice and formation of robust Pb-Cl and Cs-Cl bonds that effectively suppress Pb_{Br} defects. Supplementing these inorganic anion strategies, researchers frequently employ specialized Lewis basic molecules and polydentate chelating agents to firmly anchor the distorted lattice through organic coordination. Zhao *et al.*[102] developed a tridentate ligand 1,10-phenanthroline-5-amine (PAA) in which two pyridyl nitrogens and one amino nitrogen simultaneously coordinate with Pb^{2+} to substantially elevate the formation energies of both I_{Pb} and V_I. This reduction in defect density is consistent with density of states (DOS) calculations indicating a more robust crystalline framework. Similarly, Zhuang *et al.*[103] utilized diphenylguanidinium bromide (DPGABr) to establish strong coordination between its $-NH_2$ groups and Pb^{2+}, which shifts the defect states induced by Pb_I

toward the band edge and extends photocarrier lifetimes from 452 to 791 ns. Advancing beyond these localized coordination effects, the multifunctional small molecule 4,7-bromo-5,6-fluoro-2,1,3-phenylpropyl thiadiazole (M4) incorporates a diverse array of Br, F, and S donor groups[104]. This broad functionalization enables M4 to address multiple defect types by concurrently suppressing V_I along with both Pb_I and I_{Pb} defects to restore proper lattice coordination. Ultimately, while advanced multifunctional molecules successfully address complex arrays of chemical defects, this chemical coordination paradigm is further elevated by macroscopic molecular locking strategies that provide comprehensive structural and mechanical stabilization across the crystal surface. As previously discussed in the context of undercoordinated Pb^{2+} passivation, the polydentate DDPUD molecule exemplifies this advanced paradigm by utilizing its C=O and -F groups to simultaneously bind Pb_I centers[74]. To fully appreciate the significance of this structural evolution, it is instructive to distinguish the DDPUD molecular locking strategy from the tridentate PAA coordination mentioned above. Both approaches transcend single-site passivation through multiple functional groups to establish robust networks with metallic centers and antisite defects. However, while the PAA strategy primarily exerts a thermodynamic influence by elevating specific defect formation energies, the DDPUD approach executes a macroscopic mechanical locking effect. Beyond chemical passivation, this rigid anchoring physically locks the top interface and grain boundaries to relieve residual tensile strain, an effect that is uniquely coupled with the formation of a robust hydrophobic barrier to significantly enhance long-term environmental stability.

Surface, grain boundary, and interface defects

While atomic-scale defects are critical, their spatial distribution and aggregation at boundaries give rise to mesoscale defects that dominate non-radiative losses in polycrystalline films. These imperfections can be broadly categorized into surface defects, grain boundary defects, and interface defects located between the perovskite layer and the charge transport layers (CTL). Among these diverse regions, the external boundaries are particularly problematic. Specifically, in mixed halide perovskite films, imperfections are primarily concentrated at the surface and interface regions, where their density is approximately 100 times higher than that of the bulk defects[105,106].

Surface defects

Because the physical termination of the perovskite lattice naturally exposes a high density of undercoordinated lead centers and atomic vacancies, the diverse coordination strategies discussed previously fundamentally serve as effective surface passivation mechanisms. Illustrating this functional overlap, targeted organic molecules such as triphenylphosphine oxide (TPPO) readily coordinate with these exposed surface species to yield a marked increase in PCE[107]. Similarly, phenethylammonium bromide (PEABr) effectively modulates the surface chemistry to reduce non-radiative recombination and improve overall film stability[108]. Although these tailored molecular interventions successfully fortify the external top interface, the polycrystalline nature of perovskite thin films introduces a vast network of internal interfaces. These internal domains, commonly known as grain boundaries, are highly susceptible to defect accumulation and moisture infiltration.

Grain boundary defects

Grain boundary defects fundamentally arise from lattice misalignment and the incomplete physical fusion between adjacent crystalline domains during the film drying process. Because these internal interfaces act as primary channels for ion migration and non-radiative recombination, researchers frequently deploy tailored organic molecules and targeted inorganic salts to regulate local crystallization. A highly advanced methodology to eliminate these boundary defects involves the synergistic incorporation of the organic spacer

furan-2-ylmethanaminium chloride (FuMACl) alongside two-dimensional perovskite crystal seeds[109]. Rather than simply passivating existing imperfections, these two-dimensional seeds function as dispersed nucleation templates within the bulk precursor solution. Dynamic light scattering (DLS) measurements reveal that these templates aggregate precursor components into significantly larger clusters, substantially lowering the thermodynamic Gibbs free energy barrier for nucleation[109]. This strategically modulated crystallization produces highly crystalline and vertically oriented perovskite grains. Complementing these internal chemical engineering strategies, recent investigations have introduced an effective environmentally assisted repair protocol that utilizes controlled oxygen exposure to target specific chemical vulnerabilities at the grain boundaries. Advanced time-resolved photoemission electron microscopy (TR-PEEM) has revealed that these boundary defect clusters are predominantly composed of a high density of interstitial iodine[110]. These interstitial iodine species act as severe deep-level traps that capture photogenerated holes over an extended spatial range through a rapid diffusion-assisted process. When the fully formed perovskite film is exposed to small doses of dry air under continuous visible light illumination, the introduced oxygen specifically interacts with these interstitial iodine-rich clusters. This photochemical reaction effectively deactivates the hole-trapping capability of the interstitial iodine and neutralizes the most detrimental boundary defects. By permanently eliminating this primary channel for non-radiative recombination, this mechanism provides a robust post-crystallization refinement pathway to restore the local electronic integrity of the polycrystalline lattice. It is important to note, however, that while the oxygen-assisted repair protocol demonstrates significant efficacy for lead-based perovskites, its application is strictly precluded in narrow-bandgap tin-lead mixed systems. In these compositions, the bivalent tin cations are thermodynamically unstable and highly susceptible to rapid oxidation into the tetravalent state upon exposure to even trace amounts of oxygen. This oxidation cascade induces severe p-type self-doping and generates a high density of deep-level trap states that severely degrade carrier dynamics. Consequently, the defect management paradigm must shift when transitioning to tin-containing frameworks. Rather than relying on oxidative healing, these sensitive systems necessitate the stringent exclusion of oxygen alongside the incorporation of robust reducing agents and oxidative inhibitors. As previously highlighted, alternative strategies utilizing sacrificial metallic tin powder to reverse oxidation, or employing multifunctional organic molecules such as melamine to provide sustained coordination-driven oxidative inhibition, are essential to preserve both the structural and electronic integrity of the narrow-bandgap lattice.

Interface defects

Interface defects at the perovskite-CTL junction act as detrimental recombination centers that severely impede device efficiency. While metal oxide layers including tin dioxide (SnO_2)[111], titanium dioxide (TiO_2)[112,113], and zincite (ZnO)[114] are widely employed to enhance interfacial stability, phosphonic acid-based self-assembled monolayers such as [4-(3,6-dimethyl-9*H*-carbazol-9-yl)butyl]phosphonic acid (Me-4PACz) have emerged as superior organic alternatives that form robust chemical bonds to improve energy-level alignment. However, the practical application of Me-4PACz is frequently hindered by its polarity-induced aggregation and the resulting poor wettability of perovskite precursor solutions, which prevents the formation of a homogeneous buried interface[115]. To overcome these limitations, current research has focused on a co-self-assembled monolayer strategy. By introducing co-assembled modifiers such as 9*H*,9′*H*-[3,3′-bicarbazole]-9,9′-diylbis(butane-4,1-diyl))diphosphonic acid (DCZ-4P) and 4,4',4''-nitrilotribenzoic acid (NA), additional phosphonic acid or carboxyl anchoring groups are incorporated to strengthen interfacial bonding and optimize precursor wettability, directly inspiring researchers to develop vertical molecular bridge architectures[116,117]. Operating through a targeted bifunctional mechanism, 4-bromobenzylphosphonic acid (4Br-BPA) utilizes its phosphonic acid functional groups to anchor onto the underlying non-stoichiometric nickel oxide (NiO_x) substrate[118]. Simultaneously, strong dipole-dipole interactions between the bridging molecule and adjacent organic species induce a lateral

tightening effect that significantly densifies the transport layer. Its terminal Br atom then effectively passivates the perovskite layer by coordinating with undercoordinated Pb^{2+}. A parallel approach involves the 2,5-thiophenedicarboxylic acid (TDCA), which similarly utilizes its carboxyl group to establish firm anchoring to the NiO_x substrate while its upper functional moiety chelates undercoordinated Pb^{2+} within the perovskite lattice[119]. While co-assembled surface modifiers successfully optimize interfacial chemistry and precursor wettability at the organic layer surface, molecular bridges execute a three-dimensional stabilization mechanism. Because their compact molecular architecture allows them to physically penetrate the existing monolayer voids, they bypass the surface restriction to directly interlock the underlying metal oxide substrate with the perovskite lattice. This vertical integration not only neutralizes chemical defects across all three distinct layers but also provides a mechanical locking effect that actively resists interfacial delamination and thermal stress. Consequently, although both methodologies significantly suppress non-radiative recombination, the dual-anchoring nature of the molecular bridge provides an inherently more robust foundation for achieving superior long-term operational stability in inverted photovoltaic devices.

Extended defects

Beyond atomic and mesoscale imperfections, extended defects such as secondary phases represent macroscopic structural disruptions that undermine the overall electronic homogeneity of the perovskite film. These defects typically originate from improper crystallization kinetics or an intentional excess of precursor materials, which leads to the formation of secondary species that can either facilitate or obstruct charge transport. A particularly prominent example is the secondary phase of PbI_2, which is frequently introduced by maintaining a stoichiometric excess of approximately 5% in the precursor solution. Previous reports have consistently demonstrated that this residual PbI_2 plays a critical role in attaining high performance by effectively passivating defects at the grain boundaries and surfaces through the formation of a type-I band alignment[120,121]. However, the inherent chemical activity of excess PbI_2 introduces a significant trade-off in terms of long-term device durability[122-124]. Excessive or uncontrolled PbI_2 is highly susceptible to photodecomposition and facilitates ion migration, which ultimately results in severe device instability and pronounced hysteresis in *J-V* characteristics[125,126]. To resolve this fundamental conflict, recent work has focused on stabilizing these secondary phases through targeted chemical conversion. Zhao *et al.*[127] demonstrated a targeted strategy by doping $FAPbI_3$ perovskites with rubidium chloride (RbCl), effectively converting the reactive PbI_2 into an inactive compound identified as $(PbI_2)_2RbCl$. Unlike pure PbI_2, this RbCl-stabilized compound remains chemically inert under operational conditions while successfully maintaining the desired passivation effects[127]. This approach achieves a certified PCE of 25.6% and ensures that devices retain 80% of their initial efficiency after 500 h of thermal stress at 85 °C. While the chemical conversion of reactive secondary species represents an effective post-crystallization stabilization approach, the fundamental suppression of extended macroscopic defects can also be achieved proactively by controlling the initial crystallization kinetics. This kinetic control is particularly critical in highly reactive systems where the rapid crystallization induced by conventional antisolvents (e.g., chlorobenzene (CB)) typically generates a high density of grain boundaries and unwanted secondary phases. To address this challenge, Zhang *et al.*[128] recently introduced the green antisolvent diethyl carbonate (DEC) to regulate the solvent-antisolvent interactions during the formation of tin-based perovskite films. Time-dependent steady-state absorption analyses reveal that DEC significantly retards the solvent extraction process to provide a prolonged thermodynamic window for ordered crystal growth. This decelerated crystallization promotes a highly preferred vertical crystal orientation and dramatically enlarges the average grain size across the perovskite film. Because macroscopic grain boundaries represent the primary extended defects in polycrystalline architectures, this morphological optimization directly suppresses their formation and eliminates the associated deep-level trapping centers.

This review has highlighted the multifaceted nature of structural defects in perovskite materials and the diverse range of additive engineering strategies developed to passivate them across atomic, mesoscopic, and macroscopic length scales. Defect-selective additive engineering strategies and key functional groups for perovskite passivation are summarized in Table 1. From mitigating anion vacancies through transient Cl^- donors to suppressing antisite defects via multidentate ligands and healing grain boundaries through environmental treatments, additive engineering has proven essential for enhancing carrier dynamics, including prolonged carrier lifetimes, improved charge mobilities, and reduced non-radiative recombination losses. However, the vast chemical space of potential additives, encompassing organic cations, anions, polymers, and hybrid molecules, poses a combinatorial challenge that cannot be efficiently addressed by traditional trial-and-error approaches. Each additive interacts with multiple defect types through complex mechanisms (coordination, hydrogen bonding, electrostatic interaction), and their effects are highly sensitive to processing conditions. This complexity calls for a paradigm shift from empirical screening to rational, data-driven design. Herein lies the transformative potential of ML. By integrating high-throughput experimental data, computational simulations (e.g., density functional theory (DFT)), and structural descriptors, ML models can predict the defect-passivation efficacy of novel additives, identify synergistic combinations, and optimize processing parameters[129]. For instance, ML can correlate molecular features (e.g., electronegativity, steric effects) with passivation performance, enabling the discovery of next-generation multifunctional additives[131]. The convergence of additive engineering and ML thus represents a powerful pathway toward accelerated materials discovery, enhanced reproducibility, and ultimately, the commercialization of high-performance PSCs.

Interface engineering for enhanced stability

In high-performance PSCs, the top and buried interfaces serve as the primary conduits for charge extraction but simultaneously represent the most vulnerable frontiers for chemical degradation and structural deterioration. While the preceding sections primarily emphasized how targeted additive engineering passivates localized interfacial defects to suppress non-radiative recombination, the ultimate significance of interfacial management extends far beyond initial efficiency enhancements. By integrating these multifaceted chemical and mechanical modifications, interface engineering collectively endows devices with the exceptional operational stability required to withstand prolonged exposure to severe thermal, photonic, and environmental stressors.

Functional group bonding

To reinforce the physicochemical shield at these vulnerable boundaries, the advanced interfacial strategies previously discussed for defect passivation, including self-assembled monolayer (SAM), co-assembled surface modifiers, and vertical molecular bridges, are equally applicable and highly effective for broader stability enhancement. The fundamental logic remains consistent across these scales. Whether the objective is passivating localized interfacial imperfections or achieving comprehensive macroscopic interface engineering, establishing strong chemical interactions between the perovskite absorber and the charge transport materials is essential. Echoing the dual functional nature of the previously discussed TDCA bridging strategy, Xiong *et al.*[132] demonstrated that perfluorophenylacylamide (PFPA) effectively coordinates with Pb^{2+} through its carbonyl group and leverages strong dipole interactions to fine-tune the energy band alignment, thereby maintaining over 85% of its initial efficiency after 350 h of storage under ambient air at room temperature and 45% relative humidity. Further extending this bridging paradigm to the top electron extraction interface, Hu *et al.*[133] designed the multifunctional 3-aminomethyl-benzothiophene (3-AMBTh) to act as an efficient charge bridge. Within this architecture, the amine group selectively reacts with V_I to heal the perovskite surface, while its aromatic backbone engages in robust π-π stacking with fullerene-based electron transport layers (ETLs). This dual-action bridge effectively suppresses charge recombination and substantially extends the operational lifetime of the device, enabling it to retain > 94% of its initial efficiency after 1,000 h of storage.

Table 1. Defect-selective additive engineering strategies and key functional groups for perovskite passivation

	Defect type	Additive	Dominant functional groups	Refs.
Point defects	Anion vacancies	MACl + [Bcmim]Cl	Cl^-	[1]
		FABP	$-PO_3^{2-}$	[70]
		$PbCl_2$	Cl^-	[79]
		MACl	Cl^-	[80]
		DTABr	Br^-	[98]
	(Undercoordinated Pb^{2+})	NMACOOH	$HCOO^-$	[71]
		H3pp	O	[87]
		ATU	C=S	[88]
		DDPUD	C=O	[96]
	Cation vacancies	FABP	$-NH_3^+$	[70]
		NMACOOH	NMA^+	[71]
		2-HZP	$-NH-NH_2$	[72]
		DTABr	DTA^+	[98]
		PVP	-C(O)NH-	[99]
		KBF_4	BF_4^-	[100]
	Antisite defects	EMImCl	Cl^-	[101]
		PAA	$-C_5H_4N$, $-NH_2$	[102]
		DPGABr	$-NH_2$	[103]
		M4	-S	[104]
		DDPUD	C=O, -F	[129]
Surface defects		TPPO	P=O	[107]
		PEABr	PEA^+	[108]
Grain boundary defects		FuMACl , 4,4-difluoropiperidinehydrochloride ($(DFP)_2PbI_4$)	$-NH_2$, O	[109]
Interface defects		SnO_2	\	[111]
		TiO_2		[112,113]
		ZnO		[114]
		Me-4PACz		[130]
		2-(3,6-dimethoxy-9H-carbazol-9-yl) ethyl] phosphonic acid (MeO-2PACz)		[130]
Extended defects	Secondary phases	DEC	C=O	[128]

MACl: Methylammonium chloride; FABP: fluorinated anilinium benzylphosphonate; ATU: amidinethiourea; PVP: polyvinylpyrrolidone; PAA: 1,10-phenanthroline-5-amine; TPPO: triphenylphosphine oxide; DEC: diethyl carbonate.

Polymer/crosslinker protection

While the strategic deployment of targeted functional groups successfully mitigates localized interfacial defects through strong chemical coordination, these discrete small-molecule modifiers frequently encounter intrinsic limitations in long-term mechanical stability and thermal robustness, as their isolated operation across the boundary renders them susceptible to desorption or unwanted diffusion under continuous operational stress. To address these limitations, current research has advanced toward incorporating polymeric and crosslinking agents to construct protective architectures at the perovskite interfaces. Li *et al*.[134] introduced a polymerized small-molecular acceptor PY-IT featuring strong fused-ring planarity

and flexible rotatable linkers. Upon deposition onto the perovskite surface, the electron-rich functional groups of PY-IT, particularly its cyano and carbonyl moieties, function as Lewis bases that firmly coordinate with undercoordinated Pb^{2+}, effectively passivating defects across both the top surface and adjacent grain boundaries. Driven by its unique topological features, PY-IT spontaneously self-arranges to adopt a face-on orientation. This polymeric network not only physically seals the vulnerable perovskite boundary but also leverages its rotatable linkers to insert deeply into grain boundaries, thereby establishing a continuous electron transfer channel. Furthermore, through strong π-π interactions with the subsequent fullerene-based ETL, this multifunctional polymeric interlayer synergistically suppresses non-radiative recombination and optimizes energy-level alignment, thereby maintaining ≈80% of its initial PCE after 1,000 h of simulated 1-sun illumination under maximum power point tracking (MPPT)[134].

Hydrophobic barriers

Beyond the intrinsic chemical vulnerabilities addressed through crystallization control, such as the rapid oxidation of divalent tin, a review of the current literature reveals that the long-term operational stability of these devices is predominantly challenged by extrinsic environmental stressors. Among these, moisture remains the primary driver of severe perovskite degradation[135]. Although recent literature proposes utilizing the targeted SAM 4-(9H-carbazol-9-yl)phenylboronic acid (4PBA) to replace hygroscopic and acidic hole transport materials such as poly(3,4-ethylenedioxythiophene):poly(styrenesulphonic acid) (PEDOT:PSS), the latter remains the predominantly utilized option in narrow-bandgap tin-lead perovskite systems[136]. Proponents of 4PBA highlight that its boronic acid group provides robust coordination anchoring to eliminate acidic corrosion while its hydrophobic backbone effectively blocks moisture infiltration to extend device lifetime. However, this hydrophobicity, originating from the peripheral carbazole group, introduces a critical fabrication challenge. While constructing a formidable moisture barrier, this hydrophobic nature directly induces severe dewetting of the highly polar perovskite precursor solution at the interface. The precursor droplets readily shrink and agglomerate, causing the resulting perovskite film to exhibit numerous pinholes and extensive areas of exposed substrate. Consequently, the pursuit of enhanced interfacial stability inadvertently compromises device scalability and manufacturing reproducibility. Furthermore, the self-assembly process of molecules like 4PBA is highly sensitive to the pretreatment state of the substrate, relying heavily on the specific spatial distribution and density of surface hydroxyl groups. If the surface activation of the conductive glass substrate exhibits microscopic inhomogeneity, the organic monolayer will suffer from localized aggregation and generate unmodified voids. These spatial discontinuities inevitably allow direct physical contact between the perovskite layer and the underlying bare oxide, triggering severe interfacial non-radiative recombination and uncontrollable leakage currents. As a result, rather than improving operational efficiency, these structural imperfections degrade the *Voc* of the photovoltaic devices. Currently, the predominant approach to combat moisture-driven degradation relies on the integration of highly hydrophobic molecules. For instance, Sharma *et al.*[137] applied alkylamine hydrochlorides of varying carbon chain lengths to successfully transform the perovskite surface from a hydrophilic state to a highly hydrophobic one, thereby achieving stable operational performance for over 1,500 h under 35%-40% relative humidity conditions. However, directly employing these strongly hydrophobic species inevitably encounters the same manufacturing paradox previously discussed regarding the 4PBA monolayer. The inherent conflict between constructing a robust moisture barrier and maintaining adequate precursor wettability severely limits device scalability and manufacturing reproducibility. To overcome this fundamental bottleneck, future research should leverage ML algorithms and high-throughput computational screening to discover novel molecular alternatives that simultaneously guarantee exceptional environmental stability without sacrificing large-area film scalability and device efficiency.

Suppression of ion migration

While the implementation of robust hydrophobic architectures effectively shields the perovskite absorber from extrinsic moisture degradation, continuous solar irradiation introduces another formidable challenge. Under prolonged illumination and operating electric fields, the perovskite lattice becomes highly susceptible to intrinsic structural instability driven by ion migration[138]. Within this light-induced degradation process, volatile halide anions represent the primary mobile species. Because these migrating anions inevitably trigger severe compositional segregation and corrosive interfacial side reactions, implementing targeted anion-immobilizing additive engineering strategies represents the most fundamental approach to device stabilization. Degani *et al.*[139] introduced the additive 4-methylphenethylammonium bromide (MPEABr), which reacts with residual PbI_2 and undergoes spontaneous ion exchange driven by the thermodynamic gradient of different halide anions, inducing the *in situ* formation of mixed-halide 2D perovskite phases with a composition gradient. This effectively constrains the migration of volatile halide anions and suppresses detrimental phase segregation throughout the active layer. By immobilizing mobile ionic species through this structural design, photovoltaic devices achieve exceptional operational robustness, exhibiting stable performance during outdoor stability tracking exceeding 800 h. Expanding on this concept, Kim *et al.*[140] developed specialized zwitterionic interfacial modifiers, specifically 3-(1-pyridinio)-1-propanesulfonate. These molecules possess a high inherent dipole moment arising from their spatially separated pyridinium and sulfonate charges. By generating a robust local electrostatic field at the interface, these zwitterions establish powerful electrostatic interactions with mobile ions to effectively anchor halide anions and organic cations to their respective charged moieties. This molecular anchoring mechanism substantially elevates the activation energy barrier for ion displacement, thereby suppressing electric-field-driven ion migration and enhancing overall structural stability under severe thermal and electrical bias stress. Furthermore, while intrinsic anion immobilization remains the primary focus of these additive strategies, modern interface engineering must simultaneously address the detrimental migration of extrinsic cations. To this end, Kim *et al.*[141] designed a novel molecular hole transport material, 1,3-bis(5-(4-(bis(4-methoxyphenyl) amino)phenyl)thieno[3,2-b]thiophen-2-yl)-5-octyl-4H-thieno[3,4-c]pyrrole-4,6(5H)-dione (coded HL38). This molecule features multiple oxygen and sulfur atoms whose electron-rich functional groups serve as efficient molecular traps, enabling the coordination and capture of lithium ions derived from conventional hygroscopic dopants. By establishing strong chemical interactions with these extrinsic cations, the HL38 layer prevents the diffusion of lithium ions across the perovskite absorber and suppresses their accumulation at the opposite charge extraction boundaries. This targeted molecular immobilization enabled the unencapsulated photovoltaic devices to retain ~86% of their initial efficiency even after 1,000 h of thermal aging at 85 °C.

In summary, interfacial engineering plays a pivotal role in achieving long-term operational stability in PSCs. The representative additive engineering strategies summarized in Table 2 are synergistic in nature, rather than mutually exclusive. Looking ahead, the integration of multifunctional molecular designs and composite interfacial architectures offers a promising route toward synergistic stabilization by unifying chemical anchoring, physical shielding, hydrophobic protection, and ion regulation within a single framework. Furthermore, to accelerate the rational design of such advanced interfaces, ML is emerging as a transformative tool. By training on large datasets of molecular structures, interfacial properties, and device performance metrics, ML models can predict optimal additive candidates, identify structure-property relationships, and guide high-throughput experimental validation. This convergence of additive engineering and data-driven intelligence enables a shift from trial-and-error screening to predictive materials discovery, significantly shortening development cycles. Ultimately, the integration of interfacial stabilization with optimal energy-level alignment, scalable fabrication, and robust encapsulation, guided by machine learning, will be crucial to realizing reliable and high-performance perovskite photovoltaics for commercial deployment.

Table 2. Representative additive engineering strategies for enhanced stability in perovskite solar cells

Strategy	Component	Additive	PCE (%)	Long-term stability	Encapsulation	Refs.
Functional group bonding	CsFAMAPbBrI	PFPA	22.42	85% after 350 h at RT and RH 45%	No	[132]
	FASnI	3-AMBTh	14.53	94% after 1,000 h in N_2	No	[133]
	$FAPbI_3$	Formamidine sulfinic acid (FSA)	24.1	85% after 1,000 h in N_2 at 50-60 °C	\	[142]
Polymer/Crosslinker protection	$Cs_{0.05}(FA_{0.98}MA_{0.02})_{0.95}Pb(I_{0.98}Br_{0.02})_3$	PY-IT	23.57	80% after 1,000 h in the air	Yes	[134]
Hydrophobic barriers	CsFAMAPbSnI	4PBA	23.45	93.5% after 2,000 h in N_2 at 25 °C	No	[136]
	$FAPbI_3$	MPEABr	24.4	Stable performance after 850 h at 15-35 °C and RH between 40%-90%	Yes	[139]
Suppression of ion migration	$FAPbI_3$	LTZ	24.9	80% after 1,968 h in N_2 at 60 °C	No	[140]
	$FA_{0.9}Cs_{0.1}PbBr_{0.2}I_{2.8}$	HL38	21.98	85.9% after 1,032 h at 85 °C	\	[141]

PCE: Power conversion efficiency; PFPA: perfluorophenylacylamide; 3-AMBTh: 3-aminomethyl-benzothiophene.

Energy-level alignment tuning for optimized photovoltaic performance

Optimal device performance requires a precise thermodynamic match between the perovskite's conduction band minimum (CBM) and the lowest unoccupied molecular orbital (LUMO) of the ETL, as well as between the perovskite's valence band maximum (VBM) and the highest occupied molecular orbital (HOMO) of the hole transport layer (HTL). Mismatched energy levels give rise to interfacial energy barriers, charge accumulation, and severe non-radiative recombination, thereby limiting both photovoltaic performance and long-term stability. As illustrated in Figure 4A, the energy-level configurations of recently reported $CsPbI_xBr_{3-x}$ ($0 \le x \le 3$) films and high-efficiency CTLs[143] are shown based on selected references[144-149]. To achieve better energy-level alignment, it is important to select ETL and HTL materials matched to the bandgap of the perovskite system and incorporate suitable additive molecules to modulate the VBM and CBM of the perovskite.

Interfacial dipole engineering

A direct approach to modulate interfacial energy levels involves the introduction of molecular additives that orient dipolar groups at perovskite interfaces while simultaneously passivating interfacial defects, thereby achieving the dual benefits of energy-level tuning and defect mitigation through a single strategy. For instance, Wang *et al.*[150] introduced chloropropyltrimethoxysilane (CPS) molecules, which feature a highly electronegative chlorine atom at one terminus and a silane functional group at the other. The chlorine atoms selectively coordinate with undercoordinated Pb^{2+} at anion vacancy sites while the silane groups anchor to the perovskite surface to facilitate the formation of an ordered monolayer. This dipole layer generates a microscopic electric field oriented from the perovskite toward the HTL, inducing a downward shift in the surface vacuum level and effectively reducing the perovskite work function by 0.35 eV [Figure 4B]. Consequently, the energy barrier between the perovskite VBM and the HTL HOMO level is significantly narrowed from 0.42 to 0.01 eV [Figure 4C]. Similarly, Sung *et al.*[151] employed [2-(9H-carbazol-9-yl)ethyl]phosphonic acid (CEPA), whose phosphonic acid groups form strong coordination interactions with undercoordinated Pb^{2+} on the perovskite surface, passivating interfacial defects, while the dipole moment of the outward-oriented carbazole groups induces an upward shift in the vacuum energy level, thereby achieving dual functionality of defect mitigation and interfacial energy-level

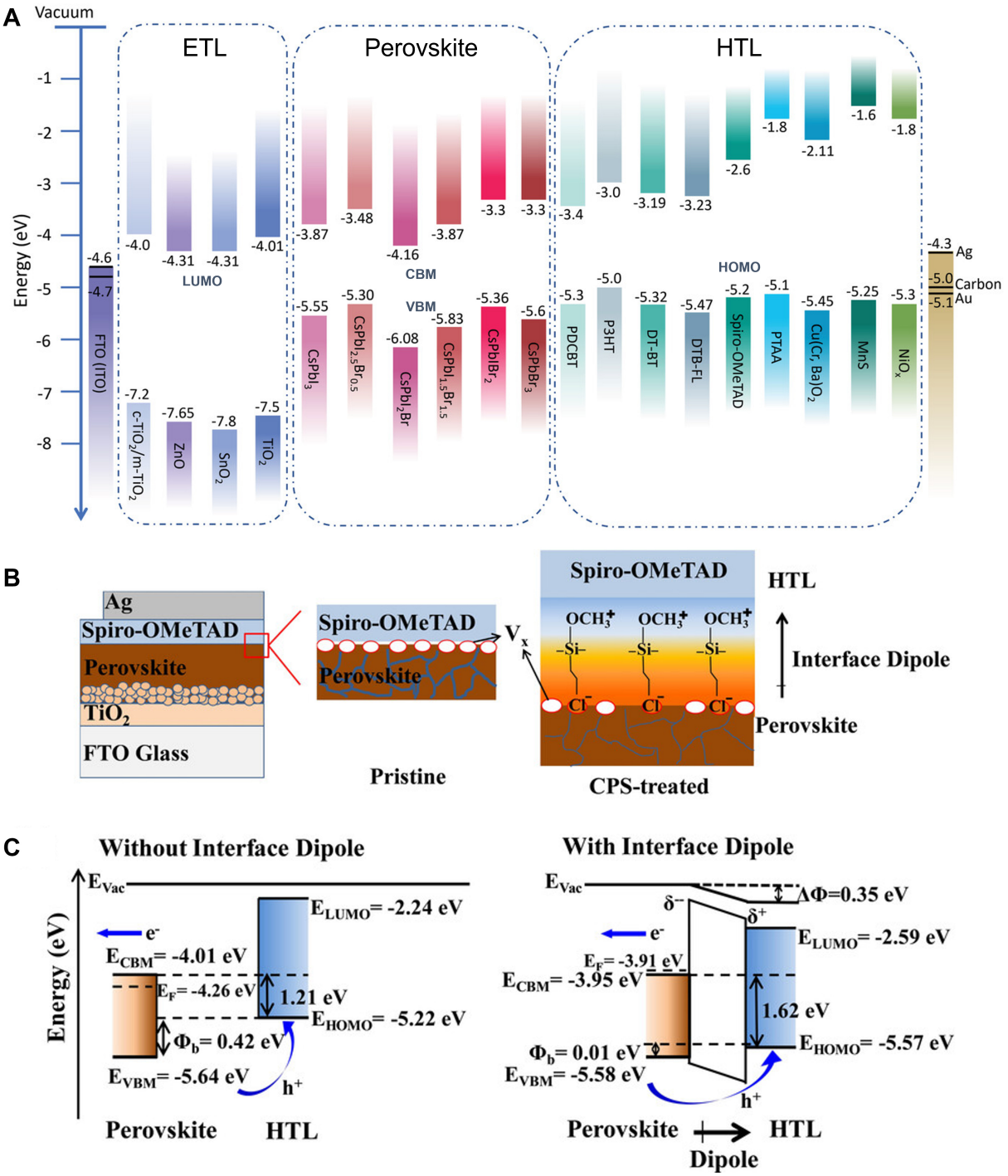

Figure 4. Schematic band diagrams of energy-level alignment. (A) Energy levels of recently reported $CsPbI_xBr_{3-x}$ ($0 \leq x \leq 3$) films and highly efficient transport layers according to refs[144-149], which were mainly obtained from absorption spectra and photoelectron spectroscopy. Note that the valence and conduction band levels as well as the work function may vary depending on the exact stoichiometry but also on the mode of preparation and surface treatments. Reprinted with permission[143]. Copyright 2022, John Wiley and Sons. (B) Schematic diagram of PSC without (central panel) and with (right panel) CPS treatment. The open red circles represent V_X sites. Reprinted with permission[150]. Copyright 2021, John Wiley and Sons. (C) Schematic band diagram of perovskite/HTL (i.e., $Cs_{0.06}FA_{0.79}MA_{0.15}Pb(I_{0.85}Br_{0.15})_3$ and Spiro-OMeTAD) without and with interfacial dipole pointing towards HTL. Note, a rigid energy shift of the HOMO and the LUMO of the HTL was assumed caused by the change in E_{Vac} after CPS treatment. Reprinted with permission[150]. Copyright 2021, John Wiley and Sons.

modulation through a single molecular design strategy. In addition to dipole engineering, the n-type characteristics of perovskite can be enhanced by incorporating additive molecules that simultaneously

passivate defects and modulate electronic properties. Liu *et al.*[152] introduced 3-(2-aminoethyl)pyridine (3-PyEA) as an additive, whose terminal amino groups react with V_{FA} on the perovskite surface while the nitrogen atoms in the pyridine ring coordinate with undercoordinated Pb^{2+} ions, effectively eliminating surface deep-level traps responsible for the p-type tendency. This dual-functional passivation restores and amplifies the n-type characteristics of the film, inducing an upward shift of the Fermi level (E_F) by 160 meV toward the CBM, thereby achieving near-optimal energy-level alignment with [6,6]-phenyl-C_{61}-butyric acid methyl ester (PCBM) and significantly improving charge extraction efficiency.

Energy cascade engineering

Constructing gradient or cascade energy steps through ultrathin interlayers represents an effective strategy for optimizing interfacial energy levels. The introduction of the hydroxylated non-fullerene acceptor NFA (IT-DOH) at the perovskite/ETL interface effectively suppresses non-radiative recombination via the specific interaction between the hydroxyl groups and undercoordinated Pb^{2+}, thereby enabling inverted PSCs to achieve superior *Voc*[153]. Crucially, intermolecular hydrogen bonding induces an expansion of the IT-DOH conjugated plane, which facilitates the formation of long-range ordered molecular packing and a preferred face-on orientation. This structural refinement provides auxiliary pathways for dissociated electrons to migrate from the perovskite to the PCBM layer, effectively minimizing energy loss during charge transport and enhancing the short-circuit current density (J_{SC}). While the vast majority of current additive engineering research focuses exclusively on improving the *Voc*, the IT-DOH strategy provides a dual enhancement of both the *Voc* and *Jsc*[154,155]. This hydroxylated non-fullerene acceptor paradigm establishes a useful foundation for future ML-guided molecular screening. On unmodified interfaces, a substantial energetic offset frequently exists between the VBM of the perovskite and the HOMO of conventional HTLs such as 2,2′,7,7′-tetrakis[N,N-di(4-methoxyphenyl)amino]-9,9′-spirobifluorene (Spiro-OMeTAD)[156]. To overcome this interfacial barrier, Shen *et al.*[157] introduced an ultrathin p-type polymeric interlayer of PDTBT2T-FTBDT (D18), which possesses a deeply situated HOMO level. By strategically positioning the D18 energy level between the perovskite valence band and the HTL, a continuous energy cascade was established. This tailored alignment enables photogenerated holes to transition smoothly along the potential gradient with negligible energy loss. Precise regulation of the D18 thickness to approximately 7 nm ensures both optimal surface coverage and effective energy-level modulation without incurring the parasitic series resistance typical of thicker polymeric films. Operating at the perovskite/HTL junction, this methodology represents a conceptual counterpart to the IT-DOH strategy employed at electron transport interfaces, further underscoring the universal efficacy of energy cascade engineering in high-performance photovoltaics. The molecular bridge strategies previously discussed in the context of interfacial defect passivation prove equally effective in facilitating superior energy-level alignment[32,76]. Although the precise mechanistic details have been discussed in the preceding sections, this dual functionality underscores a critical overarching principle in perovskite research, namely that the enhancements provided by additive engineering are not isolated but rather function through a multifaceted approach to synergistically improve the collective photovoltaic characteristics of PSCs.

In summary, achieving favorable interfacial energetics is not a standalone objective but rather a synergistic component of comprehensive defect and interface management. As evidenced by the diverse molecular interventions discussed, simultaneously addressing energy-level offsets and chemical vulnerabilities through multifunctional additives represents an effective paradigm for minimizing non-radiative losses and maximizing charge extraction in perovskite photovoltaics. Looking forward, the integration of ML with additive engineering is poised to advance the rational design of these interfacial modifiers. By systematically extracting quantum descriptors from DFT calculations, such as molecular dipole moments and binding affinities, ML algorithms can utilize these physical parameters as core input features alongside high-throughput experimental datasets[158,159]. This integration enables computational models to accurately

forecast the energy-level shifting capabilities and passivating efficacy of candidate molecules[160], accelerating the discovery of optimal passivators and energy alignment agents. Ultimately, this convergence of additive engineering and data-driven methods not only enhances molecular design precision but also establishes a predictive paradigm for interfacial energy management.

MACHINE LEARNING FOR ADDITIVE ENGINEERING IN PEROVSKITE SOLAR CELLS

Data-driven additive retrospection

As underscored throughout the preceding discussion, the role of additives in PSCs is fundamentally multidimensional, where a single molecular intervention often simultaneously influences defect density, energy-level alignment, and long-term environmental stability. This intricate interconnectedness between chemical structure and device physics implies that selecting a high-performing additive is no longer a simple task of addressing an isolated vulnerability but rather a complex multi-objective optimization process. The massive compositional and processing parameter space created by these multifunctional additives renders conventional trial-and-error methodologies increasingly inefficient. Consequently, the high dimensionality and nonlinear relationships between molecular features and device metrics make additive engineering not only highly amenable to ML approaches but also dependent on their application. Early efforts focused on uncovering empirical correlations from large experimental datasets. Odabaşı *et al.*[161] demonstrated through analysis of 1,921 PSCs that the implementation of a ternary dopant mixture comprising lithium bis(trifluoromethylsulfonyl) imide salt (LiTFSI), 4-tert-butylpyridine (TBP), and tris(2-(1H-pyrazol-1yl)-4-tert-butylpyridine) cobalt(III) tris-(bis(trifluoromethylsulfonyl)imide)) (FK209) significantly enhanced device performance, yielding a lift ratio of 2.76 for achieving stabilized PCE exceeding 18%. Quantitatively, while photovoltaic devices employing this specific dopant formulation constituted merely 8% of the entire experimental dataset, they accounted for 21% of all top-tier high-efficiency devices. In addition to evaluating specific HTL dopants, Odabaşı *et al.*[161] systematically assessed the impact of various fabrication parameters, including mixed-cation perovskite compositions, solvent engineering strategies (e.g., dimethylformamide and dimethyl sulfoxide mixtures (DMF + DMSO)), antisolvent treatments (e.g., chlorobenzene (CB)), and diverse ETL architectures incorporating tin oxide. This analysis provides robust support for optimization practices that have historically relied on empirical trial-and-error methodologies, while simultaneously laying the groundwork for a paradigm shift from heuristic screening to predictive molecular design. Despite the scale and statistical rigor of this meta-analysis, the selected parameter space exhibits several critical omissions that limit its predictive capacity for future additive development. First, continuous processing variables such as precursor concentrations, spin-coating parameters, and annealing conditions were excluded due to inherent inconsistencies in reporting standards across different laboratories. Furthermore, the ML models employed PCE as the sole target output, thereby neglecting long-term operational stability and scalability metrics, which currently represent the most pressing bottleneck in perovskite commercialization. Most critically, these algorithms were trained on discrete categorical labels rather than intrinsic physicochemical properties, such as dipole moments, binding affinities, and steric effects. Consequently, the resulting models are inherently limited to optimizing existing formulations rather than predicting entirely novel multifunctional additives, highlighting the need for more sophisticated frameworks that integrate continuous processing parameters, multidimensional stability assessments, and quantum chemical molecular descriptors.

Data-driven additive screening

To establish a more robust data-driven foundation, Wu *et al.*[41] extracted 63 experimentally validated data points from approximately 26 different molecular additives reported in the literature to construct their training dataset. Utilizing the RDKit library, they extracted 14 molecular descriptors (including molecular weight, complexity, oxygen atom count, and hydrogen bond acceptor count) and comparatively evaluated five ML models, namely linear regression (LR), random forest (RF), gradient boosting (GB), extreme

gradient boosting (XGBoost), and support vector regression (SVR). The RF model demonstrated superior performance with a test set $R^2 = 0.741$. Subsequently, they screened 141 candidate molecules from the PubChem database based on their predicted PCE enhancement ratios. Three representative molecules were selected, namely 5-carboxyphthalide (5-CP, predicted ratio = 1.218 ± 0.05) as a high-performance candidate, 4-(hydroxymethyl)benzoic acid (4-HMBA, predicted ratio = 1.101 ± 0.05) for moderate enhancement, and ethanethiol (EtSH, predicted ratio = 0.939 ± 0.05) as a potential detrimental additive. Experimental validation revealed that devices modified with 5-CP achieved a PCE of 21.4%, representing a significant enhancement compared to the 18.4% PCE of control devices, while EtSH led to a performance decline to 17.8%[41]. Although stability testing confirmed that 5-CP-modified devices exhibited superior stability relative to control samples, this observation was incidental rather than a direct prediction output of the initial ML model. Since the random forest algorithm was trained exclusively on efficiency enhancement ratios, the screening process may overlook candidate additives that provide deeper synergistic effects between photovoltaic performance and structural resilience. This limitation underscores the need for future models to incorporate multiple performance metrics to identify additives with broader benefits.

Data-driven additive prediction

Starting with a summary and preliminary screening of known additives, the ultimate objective of ML is to achieve precise prediction of device performance and directly guide experimental discovery. Yang *et al.*[162] pioneered this transition by constructing a robust predictive framework based on a large-scale historical dataset of 2,079 experimentally fabricated solar cells. Rather than analyzing parameters in isolation, their algorithm simultaneously evaluates interconnected descriptors, using experimental compositions as input features (rather than material physicochemical properties or characterizations), including precise stoichiometric ratios of chemical components and varying concentrations of specific additives, to forecast the final PCE. To validate the accuracy of the predictions, 12 independent devices were fabricated, yielding an average absolute error of merely 1.6% between the predicted and experimentally measured efficiencies, as illustrated in Figure 5.

While this impressively low error rate demonstrates strong predictive reliability, it is important to acknowledge that real-world fabrication is strongly influenced by the surrounding environment. To address the inherent risk of models overfitting to idealized laboratory conditions, Liu *et al.*[163] expanded their predictive feature matrix to encompass dynamic ambient variables such as relative humidity and processing atmosphere. Rather than treating these environmental factors as noise, a RF algorithm was deployed to capture the nonlinear interplay between precursor chemistry and atmospheric conditions, directly forecasting the resultant PCE. By incorporating atmospheric metadata into the computational framework, this methodology transforms ML from an isolated molecular screening tool into a broader predictive instrument capable of addressing the complexities of industrial-scale perovskite fabrication.

To further ensure that such computational frameworks capture generalizable physical laws rather than merely memorizing training data noise, recent methodologies have integrated interpretable frameworks with advanced molecular modeling. Liao *et al.*[164] leveraged theoretically computable, effective, and reusable molecular descriptors rather than relying on coarse structural classifications. Their approach incorporated three distinct descriptor sets, including the ground-state property descriptor set (MDS-GS, containing 23 descriptors), the absorption spectrum property descriptor set (MDS-ABS, containing 19 descriptors), and the electron transfer property descriptor set (MDS-ET, containing 5 descriptors). Furthermore, by integrating Shapley Additive exPlanations (SHAP) analysis, the researchers decoded the algorithmic black box, filtering out redundant variables and identifying the most critical physical descriptors governing device efficiency. This targeted feature selection compels the algorithms to anchor their predictions on fundamental chemical principles rather than spurious statistical correlations, thereby establishing a reliable predictive baseline. The

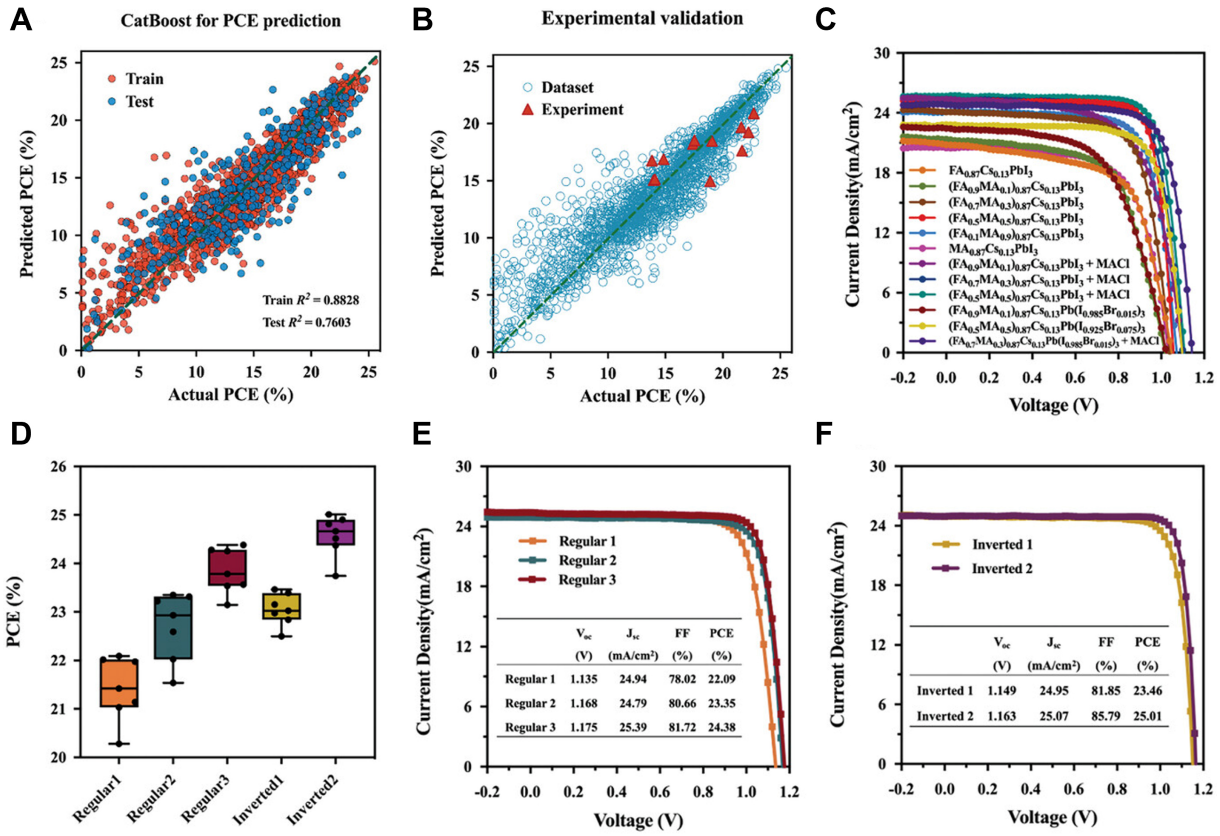

Figure 5. Machine learning model prediction and experimental photovoltaic performance of perovskite solar cells. (A) The fitting graph of PCE results by the CatBoost-based algorithm model, where red represents the training set and blue represents the test set. Reprinted with permission[162]. Copyright 2024, John Wiley and Sons. (B) The distribution of experimental results and data points from the database in the fitting graph. Reprinted with permission[162]. Copyright 2024, John Wiley and Sons. (C) *J-V* curves of devices with different perovskite components via a two-step spin-spin sequential deposition method. Reprinted with permission[162]. Copyright 2024, John Wiley and Sons. (D) Statistics of the PCE of PSCs with different groups based on 7 devices. The central line represents the median, the box limits correspond to the upper and lower quartiles, and the whiskers extend to the minimum and maximum values. Reprinted with permission[162]. Copyright 2024, John Wiley and Sons. (E) *J-V* curves of the regular devices and their champion photovoltaic performance. Reprinted with permission[162]. Copyright 2024, John Wiley and Sons. (F) *J-V* curves of the inverted devices and their champion photovoltaic performance. Reprinted with permission[162]. Copyright 2024, John Wiley and Sons.

most effective safeguard against overfitting remains rigorous out-of-sample evaluations. To validate the generalization capability of this methodology, the team conducted a blind test on 17 newly designed photovoltaic molecules. The predictive results demonstrated strong precision, achieving a mean absolute error (MAE) of only 1.02% across the test group. Notably, the PCE of 10 novel molecular candidates were predicted within a 1% error margin. This validation confirms that the model has captured the underlying structure-property relationships rather than merely interpolating within known historical data, thereby enabling rapid in silico evaluation of unexplored chemical spaces and providing a transparent and rational blueprint for the design of future functional materials.

However, the most pervasive challenge in ML-based models arises when the available experimental datasets are extremely limited. To address this small-sample bottleneck, the Co-Pilot for Perovskite Additive Screener (Co-PAS) framework was developed around a fundamental shift in data partitioning and feature representation. Pu *et al.*[165] abandoned traditional data augmentation strategies and instead focused on the physical logic of data partitioning and the transferability of dimensionality reduction techniques. To address the severe performance distortion and high variance caused by the random splitting of small datasets, they

introduced a Molecular Scaffold Classifier (MSC). This methodology categorizes the limited pool of known additives into distinct scaffold groups based on their underlying topological structures, utilizing these classifications as the basis for data segmentation. This diversity-driven partitioning compels the algorithm to learn the governing physicochemical principles of all core scaffolds during training, thereby reducing the risk of memorizing specific local features and improving generalization to entirely novel molecular architectures. Furthermore, to address the limited feature representation caused by insufficient target data, the framework deployed a transfer learning strategy using a Junction Tree Variational Autoencoder (JTVAE). Rather than training this autoencoder from scratch on the small target dataset, the algorithm was pre-trained on a massive external database comprising millions of organic compounds from ZINC. Through this approach, the framework translates complex additive structures into continuous latent vectors that encode substantial chemical prior knowledge. This molecular representation overcomes the limitations of traditional manual descriptors, granting the predictive model strong molecular analytical capabilities despite the limited volume of available device data. This integrated strategy combining physical scaffold constraints with pre-trained features demonstrated strong predictive accuracy during high-throughput screening. As the most rigorous experimental validation, the researchers applied this framework to evaluate a chemical space of 250,000 unknown molecules, successfully isolating a previously unreported additive named Boc-L-threonine N-hydroxysuccinimide ester (BTN)[165]. Subsequent device fabrication confirmed that PSCs incorporating the BTN passivation strategy achieved a PCE of 25.20%. By successfully navigating extreme data scarcity, this approach establishes a transferable methodological blueprint for future ML-guided additive engineering under conditions of limited experimental data [Figure 6].

Representative ML-driven optimization strategies for PSCs are summarized in Table 3. In summary, the integration of ML into perovskite additive engineering has demonstrated a clear evolutionary trajectory, advancing from data-driven additive analysis to high-throughput screening and ultimately toward predictive additive design. However, despite these algorithmic advancements, the majority of current predictive frameworks optimize PCE as the sole target property. This singular focus overlooks the broader requirements for commercialization, notably long-term operational stability and manufacturing feasibility. A key barrier to incorporating these critical factors into computational models is the severe lack of standardization across the research community. Experimental protocols for assessing device stability vary considerably in duration, temperature, and atmospheric exposure, while scalability metrics are complicated by diverse substrate architectures and vastly different active area dimensions. Future methodologies must prioritize unifying these disparate testing conditions to construct multidimensional target matrices, enabling algorithms to design additives that meet commercialization requirements rather than merely achieving isolated laboratory efficiency records. Furthermore, progress is also hindered by the fundamental limitations of current dataset scale, quality, and bias. Because current predictive models predominantly rely on aggregated historical literature, they are affected by survivorship bias, learning primarily from successful devices while overlooking the insights hidden within negative results. To move beyond these finite and biased historical datasets, the field must pivot toward autonomous learning paradigms.

FUTURE OUTLOOK

Future progress in PSCs will increasingly depend on the synergistic integration of ML and additive engineering. Rather than serving merely as post-hoc analytical tools, ML frameworks are poised to evolve into prescriptive design platforms capable of generating actionable molecular blueprints. The rapid advancement of deep generative models, including variational autoencoders, normalizing flows, and language model-based molecular design pipelines, enables exploration of chemical spaces that extend well beyond conventional molecular libraries[170]. By integrating such rigorous physical descriptors as formation energies for point and extended defects, solvation dynamics, and band alignment targeting the valence and conduction band edges, these models can deliver both high predictive accuracy and mechanistic

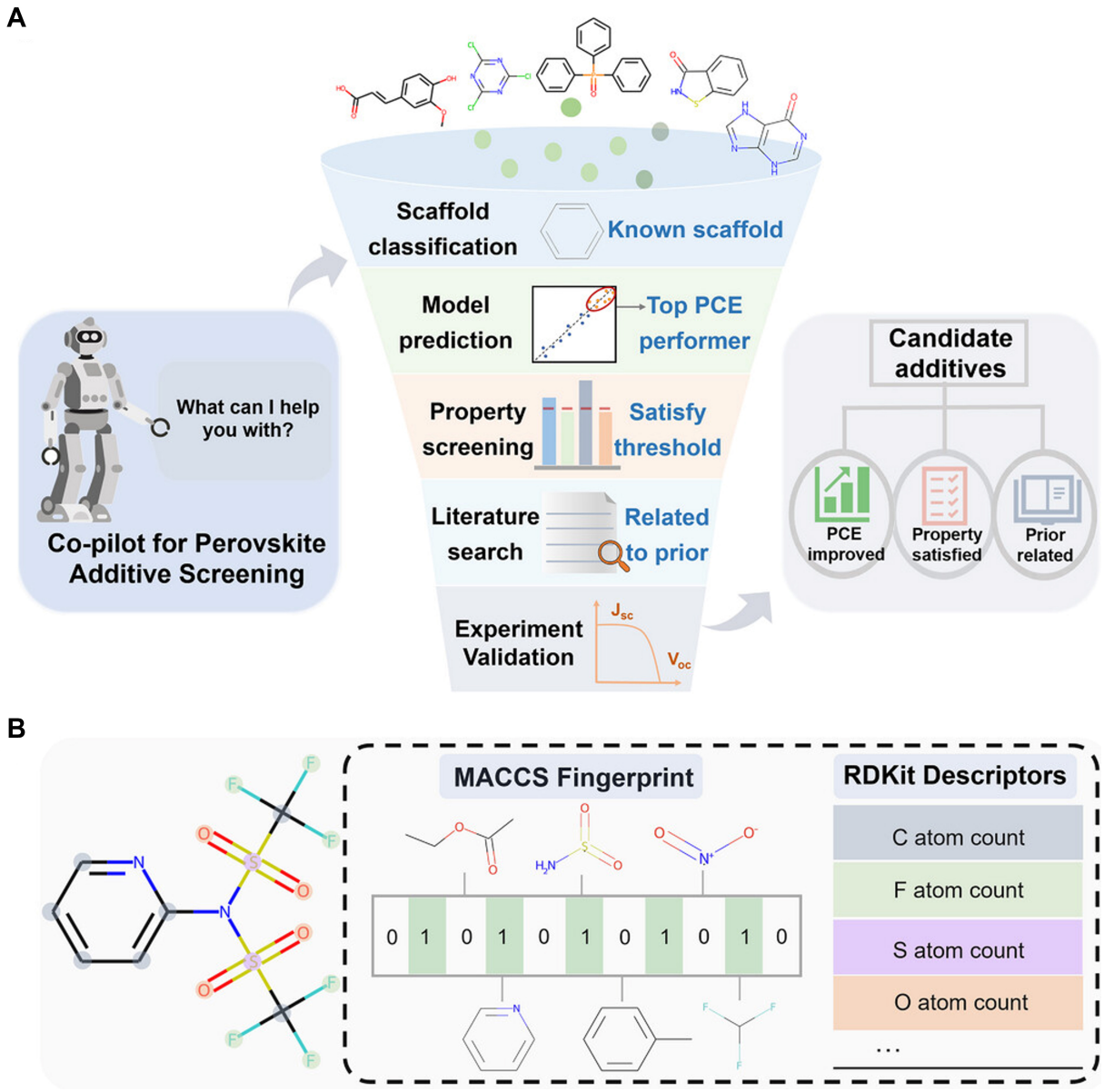

Figure 6. The data-driven Co-PAS framework and molecular encoding mechanisms for perovskite photovoltaic additive discovery. (A) Schematic of the Co-PAS workflow for screening candidate additives in PSCs. The screening process involves five steps: molecule scaffold classification, model prediction, property screening, literature search, and experiment validation. Reprinted with permission[165]. Copyright 2025, John Wiley and Sons. (B) Methods for molecular representation, including Molecular Access System (MACCS) fingerprints and RDKit molecular descriptors: MACCS fingerprints illustrate the binary encoding of molecular structures, and RDKit molecular descriptors are used to quantify various molecular features. Reprinted with permission[165]. Copyright 2025, John Wiley and Sons.

interpretability. This ensures that proposed additives are consistent with underlying physicochemical principles, shifting the paradigm from correlation to causation and marking a critical step toward physics-informed molecular discovery[171].

As perovskite photovoltaics advance toward commercialization, sustainability must become a central criterion in additive design. The field is witnessing a growing shift toward low-toxicity, biodegradable, and bio-inspired molecules, a transition that can be significantly accelerated through algorithmic screening of environmentally benign candidates. Beyond initial selection, predictive models can forecast the dynamic response of additives to environmental stressors such as moisture, oxygen and thermal cycling, enabling the

Table 3. Representative machine learning-driven optimization strategies for perovskite solar cells

Dataset sources	Algorithms	Descriptors	Target properties	Optimized additives/parameters	Experimental validation results	Refs.
Training set: 63 data points comprising 26 different molecular additives extracted from published literature; virtual screening pool: 141 candidate molecules sourced from the PubChem database	RF	Molecular weight, C atom, H atom, N atom, S atom, O atom, hydrogen bond donor, hydrogen bond donor acceptor, rotatable bond, complexity, TPSA, Ipc, MolLogP	PCE	5-CP	PCE = 21.4%	[41]
2079 data points extracted from 1,149 experimental articles published between 2013 and 2023	CatBoost	14 experimental processing factors generating 22 features including precise stoichiometric ratios precursor solutions transport layer materials and various passivating additives	PCE	2-phenylethylammonium iodide (PEAI) as HTL passivator, cuprous thiocyanate (CuSCN) doped Spiro-OMeTAD and 4-chlorobenzenesulfonate as precursor additives	PCE = 25.01%	[162]
127 data points comprising experimentally measured Zn-porphyrin-sensitized solar cells from peer reviewed literature sources	Light gradient boosting machine (LGBM), artificial neural network (ANN) and convolutional neural network (CNN)	Ground state property descriptor set (MDS-GS, containing 23 descriptors), the absorption spectrum property descriptor set (MDS-ABS, containing 19 descriptors), and the electron transfer property descriptor set (MDS-ET, containing 5 descriptors)	PCE	D58-DP-ZnP-A44	PCE = 10.5%	[164]
An initial extremely limited dataset comprising only 129 known perovskite additives extracted from literature which was subsequently utilized to systematically screen a massive library of 250,000 unknown molecules randomly drawn from PubChem	The Co-PAS framework integrating a MSC for robust structural data partitioning and a pre-trained JTVAE	Continuous high dimensional latent vectors generated by the JTVAE combined with key molecular properties including donor number dipole moment and hydrogen bond acceptor count	PCE	BTN	PCE = 25.20%	[165]
120 datasets collected from previous experiments (108 for training, 12 for validation)	RF	Nanopatterning depth of mesoporous-titanium dioxide (mp-TiO_2), weight percentage (wt%) of PCBM	*Jsc*, *Voc*, fill factor (FF), PCE	127 nm nanopatterning depth and 0.10 wt% of PCBM	PCE = 17.338%, *Jsc* = 22.877 mA cm^{-2}, *Voc* = 0.963 V, FF = 78.7%	[166]
Experimental data generated in-house, starting with initial *J-V* curves of devices doped with 0%, 4%, 8%, and 10% potassium iodide (KI), and iteratively updated with new experimental rounds	Gaussian process regression (GPR) equipped with a squared exponential kernel	KI doping concentration, voltage	PCE	3% KI doping	PCE = 20.91%	[167]
In-house generated data via a high-throughput experimental platform, the initial dataset comprised 81 fully fabricated solar cells exploring 21 ternary compositions	Multiobjective bayesian optimization (BO) utilizing Gaussian Process surrogate models and the qNEHVI acquisition function	Volume ratios of three precursor solutions including pristine $MAPbI_3$ and solutions containing 5-ammonium valeric acid iodide (AVAI) or MACl additives	Peak PCE, ΔPCE	0.14 M MACl and 0.06 M AVAI	PCE~11%, ΔPCE ~0.7%	[168]

Experimental data meticulously extracted from peer reviewed publications published between 2015 and 2024 focusing on PSCs and their passivation materials	Extreme gradient boosting (XGB)	Comprehensive multi-level features encompassing structural physical and electronic properties prominently featuring molecular fingerprints steric hindrance charge transfer distance and frontier molecular orbital energies	PCE (*Voc*)	Benzodithiophene terthiophene rhodanine derivative (BTR-Cl)	PCE = 25.36%, *Voc* = 1.186 V	[169]

PCE: Power conversion efficiency; HTL: hole transport layer; MSC: Molecular Scaffold Classifier; JTVAE: Junction Tree Variational Autoencoder; Co-PAS: co-pilot for perovskite additive screener.

rational design of environmentally stable systems that maintain structural integrity under operational conditions. A crucial next step is the integration of life-cycle assessment (LCA) metrics into computational workflows, allowing simultaneous optimization of device efficiency and environmental impact. Although currently underexplored, this approach holds significant promise for aligning photovoltaic development with the principles of green chemistry and the circular economy.

A key frontier lies in the development of multifunctional additives capable of simultaneously mitigating multiple degradation pathways, including targeted defect passivation, suppression of ion migration, and stabilization of chemically active phases. ML-driven frameworks are already demonstrating success in identifying synergistic effects within composite systems, revealing complex chemical interactions such as deprotonation and proton exchange mechanisms that are difficult to access through conventional trial-and-error approaches. Looking ahead, significant opportunities exist to expand additive discovery beyond small organic molecules to include emerging material classes such as two-dimensional nanosheets, quantum dots, covalent organic frameworks (COFs), and supramolecular assemblies. While many of these architectures remain at the proof-of-concept stage, algorithmic prediction can accelerate their maturation by linking molecular structures to multi-output device responses, paving the way for scalable solutions.

The most transformative advances are likely to emerge from closed-loop discovery paradigms that unify ML, high-throughput experimentation, and multiscale simulations. Autonomous robotic platforms have already demonstrated the feasibility of such integrated workflows, yet their specific application to additive optimization in PSCs remains early-stage[172]. By integrating ML with DFT and molecular dynamics (MD) simulations, researchers can link such atomistic descriptors as charge density distributions and vibrational spectra to macroscopic device performance metrics, thereby establishing design principles applicable across diverse fabrication protocols[173]. Future progress will hinge on scaling these integrated workflows to industrially relevant dimensions, ultimately transforming additive engineering into a self-driving materials discovery process that is both efficient and predictive. Collectively, these converging pathways will drive the technology from empirical observation to knowledge-driven innovation, accelerating the transition from laboratory breakthroughs to commercial deployment.

CONCLUSION

Additive engineering has proven indispensable in advancing PSC technology, offering a versatile toolkit to simultaneously optimize film quality, passivate defects, stabilize interfaces, and align energy levels. Through rational molecular design, additives have evolved into multifunctional agents that actively govern the perovskite formation process from the precursor solution to the final crystalline film, thereby enabling precise control over material properties and significantly enhancing device performance. Yet, the historical reliance on trial-and-error experimentation severely limits the speed and scalability of additive discovery. This challenge is being systematically addressed through the strategic integration of ML, which is transforming additive engineering into a predictive and rational science. As summarized in this review, this

transformation follows a clear evolutionary trajectory, advancing from data-driven analysis and high-throughput screening to physics-informed prediction. Despite these algorithmic advancements, several critical limitations remain. Current predictive frameworks predominantly focus on PCE as a singular target property, neglecting essential requirements such as long-term stability and industrial scalability. Furthermore, the survivorship bias inherent in historical literature datasets and the lack of standardized testing protocols continue to limit the generalization of these models. Looking ahead, the convergence of ML and additive engineering will drive the next wave of innovation in perovskite photovoltaics. Future efforts must explore broader molecular spaces using deep generative models and rigorous physical descriptors, shifting the paradigm from empirical correlation to physics-informed design. Multifunctional additive design should expand to encompass complex material architectures while incorporating sustainability through LCA and green chemistry principles. Ultimately, the most transformative advances will emerge from closed-loop discovery paradigms that unify multiscale simulations, high-throughput experimentation, and autonomous robotic platforms. By scaling these integrated workflows to industrially relevant dimensions, the field will move toward a self-driven materials discovery process, accelerating the transition of efficient, stable, and environmentally friendly PSCs from laboratory to commercial deployment.

DECLARATIONS

Authors' contributions

Performed the literature search, conducted the synthesis, and wrote the manuscript: Wang, H.
Assisted with study design: Meng, J.
Revised the manuscript for intellectual clarity: Kang, F.
Reviewed the final manuscript: Wei, G.
All authors contributed to the conceptualization of this review.

Availability of data and materials

Not applicable.

AI and AI-assisted tools statement

Not applicable.

Financial support and sponsorship

This work is supported by funding from National Natural Science Foundation of China (52027817, 52572175), Tsinghua Shenzhen International Graduate School Overseas Research Cooperation Fund (HW2024008).

Conflicts of interest

All authors declared that there are no conflicts of interest.

Ethical approval and consent to participate

Not applicable.

Consent for publication

Not applicable.

REFERENCES

1. Ding, B.; Ding, Y.; Peng, J.; et al. Dopant-additive synergism enhances perovskite solar modules. *Nature* **2024**, *628*, 299-305. DOI PubMed PMC
2. Feng, Z.; Wang, Y.; Si, J.; et al. Multi-site lead passivation via spatial configuration modulation of additives for efficient perovskite solar cells. *Adv. Energy. Mater.* **2025**, *15*, 2502409. DOI

3. Mahmud, M. A.; Duong, T.; Peng, J.; et al. Origin of efficiency and stability enhancement in high-performing mixed dimensional 2D-3D perovskite solar cells: a review. *Adv. Funct. Mater.* **2021**, *32*, 2009164. DOI
4. Zhang, J.; Tang, S.; Zhu, M.; et al. The role of grain boundaries in organic-inorganic hybrid perovskite solar cells and its current enhancement strategies: a review. *Energy. Environ. Mater.* **2024**, *7*, e12696. DOI
5. Choi, H.; Liu, X.; Kim, H. I.; Kim, D.; Park, T.; Song, S. A facile surface passivation enables thermally stable and efficient planar perovskite solar cells using a novel IDTT-based small molecule additive. *Adv. Energy. Mater.* **2021**, *11*, 2003829. DOI
6. Xiong, S.; Hou, Z.; Zou, S.; et al. Direct observation on p- to n-type transformation of perovskite surface region during defect passivation driving high photovoltaic efficiency. *Joule* **2021**, *5*, 467-80. DOI
7. Jiang, W.; Zhu, Y.; Liu, J.; et al. Improving the stability of wide bandgap perovskites: mechanisms, strategies, and applications in tandem solar cells. *Adv. Mater.* **2025**, *37*, 2418500. DOI
8. Dong, W.; Qiao, W.; Xiong, S.; et al. Surface passivation and energetic modification suppress nonradiative recombination in perovskite solar cells. *Nano. Micro. Lett.* **2022**, *14*, 108. DOI PubMed PMC
9. Song, J.; Xie, H.; Lim, E. L.; Hagfeldt, A.; Bi, D. Progress and perspective on inorganic $CsPbI_2Br$ perovskite solar cells. *Adv. Energy. Mater.* **2022**, *12*, 2201854. DOI
10. Huang, J.; Wang, H.; Jia, C.; et al. Advances in crystallization regulation and defect suppression strategies for all-inorganic $CsPbX_3$ perovskite solar sells. *Prog. Mater. Sci.* **2024**, *141*, 101223. DOI
11. Chen, P.; Xiao, Y.; Li, S.; et al. The promise and challenges of inverted perovskite solar cells. *Chem. Rev.* **2024**, *124*, 10623-700. DOI
12. Huang, Y.; Zhang, W.; Xiong, Y.; et al. Recent advancements in ambient-air fabrication of perovskite solar cells. *Exploration* **2025**, *5*, 20240121. DOI PubMed PMC
13. Kang, Y.; Li, R.; Wang, A.; et al. Ionogel-perovskite matrix enabling highly efficient and stable flexible solar cells towards fully-R2R fabrication. *Energy. Environ. Sci.* **2022**, *15*, 3439-48. DOI
14. Bellani, S.; Bartolotta, A.; Agresti, A.; et al. Solution-processed two-dimensional materials for next-generation photovoltaics. *Chem. Soc. Rev.* **2021**, *50*, 11870-965. DOI PubMed PMC
15. Kojima, A.; Teshima, K.; Shirai, Y.; Miyasaka, T. Organometal halide perovskites as visible-light sensitizers for photovoltaic cells. *J. Am. Chem. Soc.* **2009**, *131*, 6050-1. DOI
16. Green, M. A.; Dunlop, E. D.; Yoshita, M.; et al. Solar cell efficiency tables (version 66). *Prog. Photovolt.* **2025**, *33*, 795-810. DOI
17. Mali, S. S.; Patil, J. V.; Steele, J. A.; Jung, Y. H.; Nazeeruddin, M. K.; Hong, C. K. Controlled crystallization and surface engineering of mixed-halide γ-$CsPbI_2Br$ inorganic perovskites via guanidinium iodide additive in air-processed perovskite solar cells. *Mater. Today.* **2023**, *67*, 33-45. DOI
18. Shin, Y. S.; Song, J. W.; Lee, D. G.; et al. De-doping engineering for efficient and heat-stable perovskite solar cells. *Joule* **2025**, *9*, 101779. DOI
19. Chen, S.; Liu, N.; Xu, F.; Wei, G. Challenges and strategies toward future stable perovskite photovoltaics. *Solar. RRL.* **2023**, *7*, 2300479. DOI
20. Liu, Y.; Akin, S.; Hinderhofer, A.; et al. Stabilization of highly efficient and stable phase-pure $FAPbI_3$ perovskite solar cells by molecularly tailored 2D-overlayers. *Angew. Chem. Int. Ed.* **2020**, *59*, 15688-94. DOI
21. Meng, J.; Gao, Y.; Hu, J.; et al. Deuterium-substituted cations enhance perovskite solar cell efficiency and stability. *Joule* **2025**, *9*, 102031. DOI
22. Kang, B.; Yan, F. Emerging strategies for the large-scale fabrication of perovskite solar modules: from design to process. *Energy. Environ. Sci.* **2025**, *18*, 3917-54. DOI
23. Perovskite solar cells that withstand photolysis and are stable under reverse bias. *Nat. Mater.* **2024**, *23*, 739-40. DOI PubMed
24. Qiu, H.; Mativetsky, J. M. Elucidating the role of ion migration and band bending in perovskite solar cell function at grain boundaries via multimodal nanoscale mapping. *Adv. Mater. Inter.* **2021**, *8*, 2001992. DOI
25. Li, X.; Xu, Z.; Zhao, R.; et al. Multifunctional interfacial molecular bridging strategy enables efficient and stable inverted perovskite solar cells. *Adv. Mater.* **2025**, *37*, 2508352. DOI
26. Liu, W.; Chen, R.; Tan, Z.; et al. Buried interface engineering for scalable processing of high-performance inverted perovskite solar modules. *Adv. Energy. Mater.* **2024**, *15*, 2404374. DOI
27. He, J.; Sheng, W.; Yang, J.; et al. Omnidirectional diffusion of organic amine salts assisted by ordered arrays in porous lead iodide for two-step deposited large-area perovskite solar cells. *Energy. Environ. Sci.* **2023**, *16*, 629-40. DOI
28. Zhou, J.; Lv, J.; Tan, L.; et al. High-efficiency large-area perovskite solar cells via a multifunctional crystallization regulating passivation additive. *Adv. Mater.* **2025**, *37*, 2502916. DOI
29. Pandey, P.; Cho, S.; Bahadur, J.; et al. 4-Phenylthiosemicarbazide molecular additive engineering for wide-bandgap sn halide perovskite solar cells with a record efficiency over 12.2%. *Adv. Energy. Mater.* **2024**, *14*, 2401188. DOI

30. Wang, T.; Li, Y.; Cao, Q.; et al. Deep defect passivation and shallow vacancy repair *via* an ionic silicone polymer toward highly stable inverted perovskite solar cells. *Energy. Environ. Sci.* **2022**, *15*, 4414-24. DOI
31. Yu, Y.; Liu, R.; Liu, C.; Shi, X. L.; Yu, H.; Chen, Z. G. Synergetic regulation of oriented crystallization and interfacial passivation enables 19.1% efficient wide-bandgap perovskite solar cells. *Adv. Energy. Mater.* **2022**, *12*, 2201509. DOI
32. Chen, K.; Xiao, X.; Liu, J.; et al. Record-efficiency printable hole-conductor-free mesoscopic perovskite solar cells enabled by the multifunctional schiff base derivative. *Adv. Mater.* **2024**, *36*, 2401319. DOI
33. Wang, Q.; Zhu, J.; Zhao, Y.; et al. Cross-layer all-interface defect passivation with pre-buried additive toward efficient all-inorganic perovskite solar cells. *Carbon. Energy.* **2024**, *6*, e566. DOI
34. Mcmeekin, D. P.; Holzhey, P.; Fürer, S. O.; et al. Intermediate-phase engineering via dimethylammonium cation additive for stable perovskite solar cells. *Nat. Mater.* **2022**, *22*, 73-83. DOI
35. Wang, P.; Li, T.; Jin, Z.; et al. Simultaneous regulation of crystallization kinetics and Sn^{2+} oxidation suppression via moderate brønsted acid for efficient tin-based perovskite solar cells. *Adv. Energy. Mater.* **2025**, *15*, e01164. DOI
36. Zeng, F.; Kong, W.; Liang, Y.; et al. Highly stable and efficient formamidinium-based 2D ruddlesden-popper perovskite solar cells via lattice manipulation. *Adv. Mater.* **2023**, *35*, 2306051. DOI
37. Zhang, W.; Xing, C.; Song, W.; et al. Manipulation of interface recombination via multi-site passivator for efficient inverted perovskite solar cells and modules. *Adv. Mater.* **2025**, *37*, 2503954. DOI
38. Cheng, W.; He, X.; Wang, J. G.; Tian, W.; Li, L. *N*-(2-aminoethyl) acetamide additive enables phase-pure and stable α-$FAPbI_3$ for efficient self-powered photodetectors. *Adv. Mater.* **2022**, *34*, 2208325. DOI
39. Chen, H.; Liu, C.; Xu, J.; et al. Improved charge extraction in inverted perovskite solar cells with dual-site-binding ligands. *Science* **2024**, *384*, 189-93. DOI
40. Wang, J.; Pan, Y.; Zhou, Z.; et al. Bimolecular crystallization modulation boosts the efficiency and stability of methylammonium-free tin-lead perovskite and all-perovskite tandem solar cells. *Adv. Energy. Mater.* **2024**, *14*, 2402171. DOI
41. Wu, Z.; Kang, L.; Huang, T.; et al. Elevating perovskite efficiency via machine learning-assisted screening of passivators. *Chem. Eng. J.* **2024**, *499*, 156391. DOI
42. Amoroso, D.; Nasti, G.; Sutter-fella, C. M.; Villone, M. M.; Maffettone, P. L.; Abate, A. The central role of colloids to explain the crystallization dynamics of halide perovskites: a critical review. *Matter* **2024**, *7*, 2399-430. DOI
43. Pascual, J.; Flatken, M.; Félix, R.; et al. Fluoride chemistry in tin halide perovskites. *Angew. Chem. Int. Ed.* **2021**, *60*, 21583-91. DOI PubMed PMC
44. Treglia, A.; Olivati, A.; Romano, V.; et al. How shallow and deep defects drive carrier dynamics in tin-iodide perovskites. *Adv. Energy. Mater.* **2025**, *15*, 2404905. DOI
45. Nakamura, T.; Yakumaru, S.; Truong, M. A.; et al. Sn(IV)-free tin perovskite films realized by in situ Sn(0) nanoparticle treatment of the precursor solution. *Nat. Commun.* **2020**, *11*, 3008. DOI PubMed PMC
46. Liu, J.; Wang, S.; Zhu, W.; Tang, Z.; Ding, L.; Hao, F. Highly symmetric Lewis base coordinated with Sn^{2+} for reducing voltage loss and retarding oxidation in tin-halide perovskite solar cells. *Chem. Eng. J.* **2023**, *453*, 139975. DOI
47. Wang, S.; Yao, H.; Zhu, W.; et al. Stabilization of perovskite lattice and suppression of Sn^{2+}/Sn^{4+} oxidation via formamidine acetate for high efficiency tin perovskite solar cells. *Adv. Funct. Mater.* **2023**, *33*, 2215041. DOI
48. Geng, S.; Zhang, S.; Shen, N.; et al. Revealing collaborative effects of binary additives on regulating precursor crystallization toward highly efficient perovskite solar cells. *Angew. Chem. Int. Ed.* **2025**, *64*, e202424910. DOI PubMed PMC
49. Xie, L.; Liu, J.; Li, J.; et al. A deformable additive on defects passivation and phase segregation inhibition enables the efficiency of inverted perovskite solar cells over 24%. *Adv. Mater.* **2023**, *35*, 2302752. DOI
50. Chen, J.; Luo, J.; Li, Y.; et al. Spatially isomeric fulleropyrrolidines enable controlled stacking of perovskite colloids for high-performance tin-based perovskite solar cells. *Angew. Chem. Int. Ed.* **2025**, *64*, e202420150. DOI
51. Shen, X.; Gallant, B. M.; Holzhey, P.; et al. Chloride-based additive engineering for efficient and stable wide-bandgap perovskite solar cells. *Adv. Mater.* **2023**, *35*, 2211742. DOI
52. Tong, G.; Son, D. Y.; Ono, L. K.; et al. Scalable fabrication of >90 cm^2 perovskite solar modules with >1000 h operational stability based on the intermediate phase strategy. *Adv. Energy. Mater.* **2021**, *11*, 2003712. DOI
53. Xu, C.; Cheng, L.; Li, Z.; et al. Fast solidification and slow growth strategy for high-performance quasi-2D perovskite solar cells. *Adv. Energy. Mater.* **2023**, *13*, 2300168. DOI
54. Zhao, X.; Qiu, Y.; Wang, M.; et al. Regulation of buried interface through the rapid removal of PbI_2·DMSO complex for enhancing light stability of perovskite solar cells. *ACS. Energy. Lett.* **2024**, *9*, 2659-69. DOI
55. Tong, G.; Zhang, J.; Bu, T.; et al. Holistic strategies lead to enhanced efficiency and stability of hybrid chemical vapor deposition based perovskite solar cells and modules. *Adv. Energy. Mater.* **2023**, *13*, 2300153. DOI

56. Li, J.; Dagar, J.; Shargaieva, O.; et al. 20.8% slot-die coated $MAPbI_3$ perovskite solar cells by optimal DMSO-content and age of 2-ME based precursor inks. *Adv. Energy. Mater.* **2021**, *11*, 2003460. DOI
57. Zhu, Y.; Liu, X.; Sui, X.; et al. Intermediate-phase homogenization through intermolecular interactions toward reproducible fabrication of perovskite solar cells. *Adv. Energy. Mater.* **2025**, *15*, 2500536. DOI
58. Pu, X.; Cao, Q.; He, X.; et al. Synergistic crystallization kinetics modulation and deep/shallow level defect passivation via an organometallic cobaltocenium salt toward high-performance inverted perovskite solar cells. *Adv. Energy. Mater.* **2024**, *14*, 2303972. DOI
59. Liu, Z.; Ono, L. K.; Qi, Y. Additives in metal halide perovskite films and their applications in solar cells. *J. Energy. Chem.* **2020**, *46*, 215-28. DOI
60. Xu, N.; Qi, X.; Shen, Z.; et al. Point defects in metal halide perovskites. *Nat. Rev. Phys.* **2025**, *7*, 554-64. DOI
61. Ma, J.; Qin, M.; Li, P.; Han, L.; Zhang, Y.; Song, Y. Crystallization kinetics modulation and defect suppression of all-inorganic $CsPbX_3$ perovskite films. *Energy. Environ. Sci.* **2022**, *15*, 413-38. DOI
62. Shen, X.; Kang, K.; Yu, Z.; et al. Passivation strategies for mitigating defect challenges in halide perovskite light-emitting diodes. *Joule* **2023**, *7*, 272-308. DOI
63. Isikgor, F. H.; Zhumagali, S.; T. Merino LV, De Bastiani M, Mcculloch I, De Wolf S. Molecular engineering of contact interfaces for high-performance perovskite solar cells. *Nat. Rev. Mater.* **2022**, *8*, 89-108. DOI
64. Li, B.; Wang, X.; Zhang, T.; et al. Silicon nitride nanocomposites at the buried interface for stable perovskite solar cells. *Nat. Photonics.* **2026**, *20*, 280-6. DOI
65. Zhang, H.; Pfeifer, L.; Zakeeruddin, S. M.; Chu, J.; Grätzel, M. Tailoring passivators for highly efficient and stable perovskite solar cells. *Nat. Rev. Chem.* **2023**, *7*, 632-52. DOI PubMed
66. Park, J.; Walsh, A. Modeling grain boundaries in polycrystalline halide perovskite solar cells. *Annu. Rev. Condens. Matter. Phys.* **2021**, *12*, 95-109. DOI
67. Su, G.; Yu, R.; Dong, Y.; et al. Crystallization regulation and defect passivation for efficient inverted wide-bandgap perovskite solar cells with over 21% efficiency. *Adv. Energy. Mater.* **2023**, *14*, 2303344. DOI
68. Gu, H.; Zhu, A.; Xia, J.; et al. Nanoscale phase management of the 2D/3D heterostructure toward efficient perovskite solar cells. *Sci. Bull.* **2024**, *69*, 2853-61. DOI
69. Zhang, H.; Tian, Q.; Xiang, W.; et al. Tailored cysteine-derived molecular structures toward efficient and stable inorganic perovskite solar cells. *Adv. Mater.* **2023**, *35*, 2301140. DOI
70. Rana, P. J. S.; Febriansyah, B.; Koh, T. M.; et al. Molecular locking with all-organic surface modifiers enables stable and efficient slot-die-coated methyl-ammonium-free perovskite solar modules. *Adv. Mater.* **2023**, *35*, 2210176. DOI
71. Zheng, L.; Shen, L.; Fang, Z.; et al. Reducing the surface reactivity of alkyl ammonium passivation molecules enables highly efficient perovskite solar cells. *Adv. Energy. Mater.* **2023**, *13*, 2301066. DOI
72. Qu, S.; Li, Y.; Huang, H.; et al. Unveiling the mutual promotion mechanism of adjacent vacancy defects enables high-performance perovskite solar cells. *Adv. Mater.* **2025**, *37*, 2508643. DOI
73. Yao, Z.; Xu, Z.; Zhao, W.; et al. Enhanced efficiency of inorganic $CsPbI_{3-x}Br_x$ perovskite solar cell via self-regulation of antisite defects. *Adv. Energy. Mater.* **2021**, *11*, 2100403. DOI
74. Liu, B.; Ren, X.; Li, R.; et al. Stabilizing top interface by molecular locking strategy with polydentate chelating biomaterials toward efficient and stable perovskite solar cells in ambient air. *Adv. Mater.* **2024**, *36*, 2312679. DOI
75. Li, M.; Ma, X.; Fu, J.; et al. Molecularly tailored perovskite/poly(3-hexylthiophene) interfaces for high-performance solar cells. *Energy. Environ. Sci.* **2024**, *17*, 5513-20. DOI
76. Chen, G.; Gan, Y.; Wang, S.; et al. Dicyandiamide-driven tailoring of the n-value distribution and interface dynamics for high-performance ACI 2D perovskite solar cells. *Nano. Micro. Lett.* **2025**, *17*, 305. DOI PubMed PMC
77. Wu, Y.; Wang, Q.; Chen, Y.; Qiu, W.; Peng, Q. Stable perovskite solar cells with 25.17% efficiency enabled by improving crystallization and passivating defects synergistically. *Energy. Environ. Sci.* **2022**, *15*, 4700-9. DOI
78. Guan, H.; Fu, S.; Zeng, G.; et al. Efficient 1.77 eV-bandgap perovskite and all-perovskite tandem solar cells enabled by long-alkyl phosphonic acid. *Energy. Environ. Sci.* **2024**, *17*, 8219-27. DOI
79. Stone, K. H.; Gold-parker, A.; Pool, V. L.; et al. Transformation from crystalline precursor to perovskite in $PbCl_2$-derived $MAPbI_3$. *Nat. Commun.* **2018**, *9*, 3458. DOI PubMed PMC
80. Kim, M.; Kim, G.; Lee, T. K.; et al. Methylammonium chloride induces intermediate phase stabilization for efficient perovskite solar cells. *Joule* **2019**, *3*, 2179-92. DOI
81. Lim, J.; Kim, J.; Davies-jones, J.; et al. Benign methylformamidinium byproduct induced by cation heterogeneity inhibits local formation of δ-phase perovskites. *Energy. Environ. Sci.* **2024**, *17*, 9134-43. DOI

82. Ma, Y.; Cai, H.; Liu, Y.; et al. Alleviation of precursor degradation induced by DMF/DMSO mixture for enhanced performance of perovskite solar cells. *Angew. Chem. Int. Ed.* **2025**, *64*, e202504253. DOI
83. Yang, T.; Gao, L.; Lu, J.; et al. One-stone-for-two-birds strategy to attain beyond 25% perovskite solar cells. *Nat. Commun.* **2023**, *14*, 839. DOI PubMed PMC
84. Su, Y.; Ding, J.; Zhang, Z.; et al. Chemical inhibition of light-induced decomposition by hindered amine for efficient and stable perovskite solar cells. *eScience* **2026**, *6*, 100451. DOI
85. Zhang, N.; Li, T.; Wang, C.; et al. Host-guest complexation strategy for passivating Pb-dimer related defects in perovskite photovoltaics. *Adv. Funct. Mater.* **2023**, *33*, 2300830. DOI
86. Ahmed, R.; Rehman, S.; Chen, Z.; Ye, F.; Ren, X. Ligand assisted hydrogen bonding: a game-changer in lead passivation and stability in perovskite solar cells. *Angew. Chem. Int. Ed.* **2024**, *137*, e202418763. DOI
87. Wang, Y.; Cao, Q.; Xiang, X.; Zhou, J. Symmetric polar molecule optimized buried interface for stable flexible perovskite solar cells. *ACS. Sustain. Chem. Eng.* **2024**, *12*, 18265-75. DOI
88. Wang, K.; Yu, B.; Lin, C.; Yao, R.; Yu, H.; Wang, H. Constructing stable perovskite with small molecule bridge interface passivation. *Adv. Energy. Mater.* **2025**, *15*, 2405571. DOI
89. Tong, X.; Ma, Y.; Xie, L.; et al. Regulating spatial charge distribution of multisite passivating additives enables stable perovskite solar cells. *Adv. Funct. Mater.* **2025**, *35*, e11458. DOI
90. Xu, T.; Xiang, W.; Ru, X.; et al. Enhancing stability and efficiency of inverted inorganic perovskite solar cells with in-situ interfacial cross-linked modifier. *Adv. Mater.* **2024**, *36*, 2312237. DOI
91. Cao, S.; Luo, S.; Zheng, T.; et al. Hybrid self-assembled molecular interlayers for efficient and stable inverted perovskite solar cells. *Adv. Energy. Mater.* **2025**, *15*, 2405367. DOI
92. Wei, H.; Chen, R.; Yang, Y.; et al. Dihydrazide-mediated crystal engineering and precursor anti-aging for efficient and stable perovskite solar cells and modules. *Adv. Funct. Mater.* **2025**, *36*, e16987. DOI
93. Liu, C.; Su, H.; Pu, Y.; et al. 3D polydentate complexing agents for passivating defects and modulating crystallinity for high-performance perovskite solar cells. *Adv. Funct. Mater.* **2023**, *33*, 2212577. DOI
94. Cheng, M.; Duan, Y.; Zhang, D.; et al. Tailoring buried interface and minimizing energy loss enable efficient narrow and wide bandgap inverted perovskite solar cells by aluminum glycinate based organometallic molecule. *Adv. Mater.* **2025**, *37*, 2419413. DOI
95. Xie, Z.; Duan, Y.; Cheng, M.; et al. High-efficiency perovskite solar cells enabled by guanylation reaction for removing MACl residual and in-situ forming 2D perovskite. *Angew. Chem. Int. Ed.* **2025**, *64*, e202419070. DOI
96. Xie, H.; Wang, Z.; Chen, Z.; et al. Decoupling the effects of defects on efficiency and stability through phosphonates in stable halide perovskite solar cells. *Joule* **2021**, *5*, 1246-66. DOI
97. Liu, Y.; Xu, H.; Ji, S.; et al. Thiourea derivative induced crystallization for enhanced efficiency and stability of perovskite solar cells over 25%. *J. Energy. Chem.* **2025**, *108*, 109-17. DOI
98. Wang, X.; Wang, Y.; Chen, Y.; Liu, X.; Zhao, Y. Efficient and stable $CsPbI_3$ inorganic perovskite photovoltaics enabled by crystal secondary growth. *Adv. Mater.* **2021**, *33*, 2103688. DOI
99. Pasha, A.; Pramanik, P.; George, J. K.; et al. Cationic and anionic vacancy healing for suppressed halide exchange and phase segregation in perovskite solar cells. *ACS. Energy. Lett.* **2023**, *8*, 3081-7. DOI
100. Cheng, H.; Liu, C.; Zhuang, J.; et al. KBF_4 additive for alleviating microstrain, improving crystallinity, and passivating defects in inverted perovskite solar cells. *Adv. Funct. Mater.* **2022**, *32*, 2204880. DOI
101. Zhu, J.; He, B.; Zhang, W.; et al. Defect-dependent crystal plane control on inorganic $CsPbBr_3$ film by selectively anchoring (pseudo-) halide anions for 1.650 V voltage perovskite solar cells. *Adv. Funct. Mater.* **2022**, *32*, 2206838. DOI
102. Zhao, W.; Guo, P.; Su, J.; et al. Synchronous passivation of defects with low formation energies via terdentate anchoring enabling high performance perovskite solar cells with efficiency over 24%. *Adv. Funct. Mater.* **2022**, *32*, 2200534. DOI
103. Zhuang, J.; Liu, C.; Kang, B.; et al. Rapid surface reconstruction in air-processed perovskite solar cells by blade coating. *Adv. Mater.* **2023**, *36*, 2309869. DOI
104. Qiao, X.; Zhu, R.; Yan, D.; et al. Multi-point collaborative passivation of surface defects for efficient and stable perovskite solar cells. *Adv. Funct. Mater.* **2024**, *34*, 2409852. DOI
105. Park, N.; Zhu, K. Scalable fabrication and coating methods for perovskite solar cells and solar modules. *Nat. Rev. Mater.* **2020**, *5*, 333-50. DOI
106. Liu, J.; Zheng, D.; Wang, K.; et al. Evolutionary manufacturing approaches for advancing flexible perovskite solar cells. *Joule* **2024**, *8*, 944-69. DOI
107. Li, C.; Vincze, A.; Park, H.; et al. Anchoring ligand engineering enables highly stable MA-free perovskite solar cells with a minimal V_{OC} deficit of 0.32 V. *Energy. Environ. Sci.* **2025**, *18*, 7660-8. DOI

108. Zhou, W.; Cai, Y.; Wan, S.; et al. A universal strategy for defects and interface management enables highly efficient and stable inverted perovskite solar cells. *Energy. Environ. Sci.* **2025**, *18*, 3828-38. DOI
109. Song, Z.; Zou, Y.; Gao, Y.; et al. Buried and bulk synergistic engineering enables high-performance inverted 2D/3D perovskite solar cells. *Energy. Environ. Sci.* **2025**, *18*, 3740-9. DOI
110. Kosar, S.; Winchester, A. J.; Doherty, T. A. S.; et al. Unraveling the varied nature and roles of defects in hybrid halide perovskites with time-resolved photoemission electron microscopy. *Energy. Environ. Sci.* **2021**, *14*, 6320-8. DOI PubMed PMC
111. Ansari, F.; Zheng, L.; Pfeifer, L.; et al. Dopamine dopes the performance of perovskite solar cells. *Adv. Mater.* **2025**, *37*, 2501075. DOI
112. Yang, H.; Zhao, J.; Ren, X.; et al. Bifunctional passivation by lewis-base molecules for efficient printable mesoscopic perovskite solar cells. *J. Energy. Chem.* **2024**, *96*, 177-84. DOI
113. Xiao, G.; Meng, R.; Yang, S.; Cao, J.; Tang, Y. Cerium oxide nanoparticle as interfacial modifier for efficient and UV-stable perovskite solar cells. *Chem. Eng. J.* **2023**, *462*, 142047. DOI
114. Fahim, M.; Firdous, I.; Daoud, W. A. Cascade bridge interfacial design for stable and sustainable flexible perovskite solar cells. *SusMat* **2025**, *5*, e70016. DOI
115. Luo, Z.; Tang, L.; Zeng, L.; et al. Albendazole passivation in inverted wide-bandgap perovskite solar cells toward efficient perovskite/$CuInGaSe_2$ tandem photovoltaics. *Adv. Mater.* **2025**, *37*, e05597. DOI
116. Chen, J.; Wang, X.; Wang, T.; et al. Determining the bonding-degradation trade-off at heterointerfaces for increased efficiency and stability of perovskite solar cells. *Nat. Energy.* **2025**, *10*, 181-90. DOI
117. Liu, S.; Li, J.; Xiao, W.; et al. Buried interface molecular hybrid for inverted perovskite solar cells. *Nature* **2024**, *632*, 536-42. DOI
118. Gao, M.; Ou, Z.; Wang, C.; et al. Multifunctional buried molecule-bridge for high-performance inverted perovskite solar cells. *Adv. Mater.* **2025**, *38*, e14273. DOI
119. Li, L.; Xue, T.; Yuan, F.; et al. Buried interface chelating molecular bridge strategy enables highly efficient and stable inverted perovskite solar cells. *Adv. Mater.* **2025**, *38*, e18406. DOI
120. Park, B.; Kedem, N.; Kulbak, M.; et al. Understanding how excess lead iodide precursor improves halide perovskite solar cell performance. *Nat. Commun.* **2018**, *9*, 3301. DOI PubMed PMC
121. Wang, H.; Wang, Z.; Yang, Z.; et al. Ligand-modulated excess PbI_2 nanosheets for highly efficient and stable perovskite solar cells. *Adv. Mater.* **2020**, *32*, 2000865. DOI
122. Liang, J.; Wang, T.; Jia, Y.; et al. Turning waste into treasure: pretreatment strategy for promoting secondary grain growth by reusing excess lead iodide in perovskite solar cells. *Adv. Mater.* **2025**, *37*, 2508211. DOI
123. Gao, Y.; Ren, F.; Sun, D.; et al. Elimination of unstable residual lead iodide near the buried interface for the stability improvement of perovskite solar cells. *Energy. Environ. Sci.* **2023**, *16*, 2295-303. DOI
124. Wang, K. L.; Li, M.; Lou, Y. H.; et al. Aniline sulfonic acid induced uniform perovskite film for large-scale photovoltaics. *Adv. Energy. Mater.* **2023**, *13*, 2203471. DOI
125. Holovský, J.; Peter, Amalathas. A.; Landová, L.; et al. Lead halide residue as a source of light-induced reversible defects in hybrid perovskite layers and solar cells. *ACS. Energy. Lett.* **2019**, *4*, 3011-7. DOI
126. Fu, S.; Sun, N.; Chen, H.; et al. On-demand formation of Lewis bases for efficient and stable perovskite solar cells. *Nat. Nanotechnol.* **2025**, *20*, 772-8. DOI
127. Zhao, Y.; Ma, F.; Qu, Z.; et al. Inactive $(PbI_2)_2$ RbCl stabilizes perovskite films for efficient solar cells. *Science* **2022**, *377*, 531-4. DOI
128. Zhang, Z.; Huang, Y.; Wang, C.; et al. Green-antisolvent-regulated distribution of p-type self-doping enables tin perovskite solar cells with an efficiency of over 14%. *Energy. Environ. Sci.* **2023**, *16*, 3430-40. DOI
129. Xu, J.; Chen, H.; Grater, L.; et al. Anion optimization for bifunctional surface passivation in perovskite solar cells. *Nat. Mater.* **2023**, *22*, 1507-14. DOI
130. Azam, M.; Du, T.; Wan, Z.; et al. Dual functionality of charge extraction and interface passivation by self-assembled monolayers in perovskite solar cells. *Energy. Environ. Sci.* **2024**, *17*, 6974-7016. DOI
131. Pu, Y.; Dai, Z.; Zhou, Y.; et al. Machine learning co-pilot for screening of organic molecular additives for perovskite solar cells. *arXiv* **2024**, 2412.14109. DOI
132. Xiong, S.; Hou, Z.; Dong, W.; et al. Additive-induced synergies of defect passivation and energetic modification toward highly efficient perovskite solar cells. *Adv. Energy. Mater.* **2021**, *11*, 2101394. DOI
133. Hu, F.; Chen, C. H.; Teng, T. Y.; et al. Constructing charge bridge path for high-performance tin perovskite photovoltaics. *Adv. Energy. Mater.* **2024**, *14*, 2302926. DOI
134. Li, D.; Huang, Y.; Ma, R.; et al. Surface regulation with polymerized small molecular acceptor towards efficient inverted perovskite solar cells. *Adv. Energy. Mater.* **2023**, *13*, 2204247. DOI

135. Azmi, R.; Zhumagali, S.; Bristow, H.; et al. Moisture-resilient perovskite solar cells for enhanced stability. *Adv. Mater.* **2023**, *36*, 2211317. DOI
136. Zhang, X.; Pascual, J.; Li, Z.; et al. Buried hole-selective interface engineering for high-efficiency tin-lead perovskite solar cells with enhanced interfacial chemical stability. *Sci. Bull.* **2025**, *70*, 556-62. DOI
137. Sharma, B.; Garai, R.; Afroz, M. A.; et al. Enhancing light utilization efficiency of semi-transparent perovskite solar cells via tailored interfacial engineering. *Adv. Energy. Mater.* **2024**, *14*, 2402473. DOI
138. Zhu, H.; Teale, S.; Lintangpradipto, M. N.; et al. Long-term operating stability in perovskite photovoltaics. *Nat. Rev. Mater.* **2023**, *8*, 569-86. DOI
139. Degani, M.; Pallotta, R.; Pica, G.; et al. Compositional gradient of mixed halide 2D perovskite interface boosts outdoor stability of highly efficient perovskite solar cells. *Adv. Energy. Mater.* **2024**, *15*, 2404469. DOI
140. Kim, H.; Choi, K.; Yoon, G. W.; et al. Modulating molecular interaction of zwitterion toward rational interface engineering of perovskite solar cells. *Adv. Energy. Mater.* **2024**, *14*, 2401263. DOI
141. Kim, S. G.; Le, T. H.; De, Monfreid. T.; Goubard, F.; Bui, T. T.; Park, N. G. Capturing mobile lithium ions in a molecular hole transporter enhances the thermal stability of perovskite solar cells. *Adv. Mater.* **2021**, *33*, 2007431. DOI
142. Qin, Z.; Chen, Y.; Wang, X.; et al. Zwitterion-functionalized SnO_2 substrate induced sequential deposition of black-phase $FAPbI_3$ with rearranged PbI_2 residue. *Adv. Mater.* **2022**, *34*, 2203143. DOI
143. Yuan, Y.; Yan, G.; Hong, R.; Liang, Z.; Kirchartz, T. Quantifying efficiency limitations in all-inorganic halide perovskite solar cells. *Adv. Mater.* **2022**, *34*, 2108132. DOI PubMed
144. Tian, J.; Xue, Q.; Yao, Q.; Li, N.; Brabec, C. J.; Yip, H. L. Inorganic halide perovskite solar cells: progress and challenges. *Adv. Energy. Mater.* **2020**, *10*, 2000183. DOI
145. Liu, T.; Zhang, J.; Qin, M.; et al. Modifying surface termination of $CsPbI_3$ grain boundaries by 2D perovskite layer for efficient and stable photovoltaics. *Adv. Funct. Mater.* **2021**, *31*, 2009515. DOI
146. Yu, B.; Shi, J.; Tan, S.; et al. Efficient (>20 %) and stable all-inorganic cesium lead triiodide solar cell enabled by thiocyanate molten salts. *Angew. Chem. Int. Ed.* **2021**, *60*, 13436-43. DOI
147. Wang, P.; Wang, H.; Mao, Y.; et al. Organic ligands armored ZnO enhances efficiency and stability of $CsPbI_2Br$ perovskite solar cells. *Adv. Sci.* **2020**, *7*, 2000421. DOI PubMed PMC
148. Niu, T.; Zhu, W.; Zhang, Y.; et al. D-A-π-A-D-type dopant-free hole transport material for low-cost, efficient, and stable perovskite solar cells. *Joule* **2021**, *5*, 249-69. DOI
149. Zhang, W.; Xiong, J.; Li, J.; Daoud, W. A. Organic dye passivation for high-performance all-inorganic $CsPbI_{1.5}Br_{1.5}$ perovskite solar cells with efficiency over 14%. *Adv. Energy. Mater.* **2020**, *11*, 2003585. DOI
150. Wang, B.; Li, H.; Dai, Q.; et al. Robust molecular dipole-enabled defect passivation and control of energy-level alignment for high-efficiency perovskite solar cells. *Angew. Chem. Int. Ed.* **2021**, *60*, 17664-70. DOI
151. Sung, S. J.; Im, J.; Kim, G.; et al. Molecular engineering for function-tailored interface modifier in high-performance perovskite solar cells. *Adv. Energy. Mater.* **2022**, *12*, 2200758. DOI
152. Liu, S.; Sun, Z.; Lei, X.; et al. Stable surface contact with tailored alkylamine pyridine derivatives for high-performance inverted perovskite solar cells. *Adv. Mater.* **2024**, *37*, 2415100. DOI
153. Yang, Q.; Liu, X.; Yu, S.; et al. Hydroxylated non-fullerene acceptor for highly efficient inverted perovskite solar cells. *Energy. Environ. Sci.* **2021**, *14*, 6536-45. DOI
154. Guan, H.; Zhou, S.; Fu, S.; et al. Regulating crystal orientation via ligand anchoring enables efficient wide-bandgap perovskite solar cells and tandems. *Adv. Mater.* **2023**, *36*, 2307987. DOI
155. Liu, D.; Chen, C.; Wang, X.; et al. Enhanced quasi-fermi level splitting of perovskite solar cells by universal dual-functional polymer. *Adv. Mater.* **2023**, *36*, 2310962. DOI
156. Dong, Y.; Rombach, F. M.; Min, G.; et al. Dopant-induced interactions in spiro-OMeTAD: advancing hole transport for perovskite solar cells. *Mater. Sci. Eng. R. Rep.* **2025**, *162*, 100875. DOI
157. Shen, L.; Song, P.; Jiang, K.; et al. Ultrathin polymer membrane for improved hole extraction and ion blocking in perovskite solar cells. *Nat. Commun.* **2024**, *15*, 10908. DOI PubMed PMC
158. Cai, Y.; Bai, Z.; Chen, C.; et al. Machine learning prediction of small molecule passivators and their impacts on the passivation and photocatalytic performance of organic-inorganic hybrid perovskite interfaces. *Energy. Mater.* **2025**, *5*, 500043. DOI
159. Liu, J.; Lv, H.; Wang, P.; et al. Synergistic machine learning and DFT screening strategy: accelerating discovery of efficient perovskite passivators. *J. Energy. Chem.* **2026**, *112*, 56-63. DOI
160. Lyu, Y.; Zhou, Y.; Zhang, Y.; et al. Fingerprinting organic molecules for the inverse design of two-dimensional hybrid perovskites with target energetics. *Sci. Adv.* **2026**, *12*, eaeb4144. DOI PubMed PMC

161. Odabaşı, Ç.; Yıldırım, R. Performance analysis of perovskite solar cells in 2013-2018 using machine-learning tools. *Nano. Energy.* **2019**, *56*, 770-91. DOI
162. Yang, A.; Sun, Y.; Zhang, J.; et al. Enhancing power conversion efficiency of perovskite solar cells through machine learning guided experimental strategies. *Adv. Funct. Mater.* **2024**, *35*, 2410419. DOI
163. Liu, T.; Evans, N.; Ji, K.; et al. Disentangling environmental effects on perovskite solar cell performance via interpretable machine learning. *ACS. Energy. Lett.* **2026**, *11*, 1609-17. DOI
164. Liao, J. M.; Chen, Y. H.; Lee, H. W.; et al. Advanced high-throughput rational design of porphyrin-sensitized solar cells using interpretable machine learning. *Adv. Sci.* **2024**, *11*, 2407235. DOI PubMed PMC
165. Pu, Y.; Dai, Z.; Zhou, Y.; et al. Data-driven molecular encoding for efficient screening of organic additives in perovskite solar cells. *Adv. Funct. Mater.* **2025**, *36*, e06672. DOI
166. Sanimu, S. N.; Yang, H. Y.; Kandel, J.; et al. Machine learning-assisted fabrication of PCBM-perovskite solar cells with nanopatterned TiO_2 layer. *Energy. Environ. Mater.* **2023**, *7*, e12676. DOI
167. Jiang, S.; Wu, C. C.; Li, F.; et al. Machine learning (ML)-assisted optimization doping of KI in $MAPbI_3$ solar cells. *Rare. Metals.* **2020**, *40*, 1698-707. DOI
168. Miftahullatif, E. B.; Pethe, S. D.; Low, A. K. Y.; et al. Machine-learning-driven in-device optimization of all-printed perovskite solar cells. *ACS. Energy. Lett.* **2025**, *10*, 3952-61. DOI
169. Lou, Q.; Wang, J.; Nie, Z.; et al. Prediction and fine screening of small molecular passivation materials for high-efficiency perovskite solar cells via an enhanced machine learning workflow. *Adv. Funct. Mater.* **2025**, *35*, e11549. DOI
170. Zhang, J.; Wu, J.; Le, Corre. V. M.; Hauch, J. A.; Zhao, Y.; Brabec, C. J. Advancing perovskite photovoltaic technology through machine learning-driven automation. *InfoMat* **2025**, *7*, e70005. DOI
171. Tao, Q.; Xu, P.; Li, M.; Lu, W. Machine learning for perovskite materials design and discovery. *NPJ. Comput. Mater.* **2021**, *7*, 23. DOI
172. Zhang, J.; Le, Corre. V. M.; Wu, J.; et al. Autonomous optimization of air-processed perovskite solar cell in a multidimensional parameter space. *Adv. Energy. Mater.* **2025**, *15*, 2404957. DOI
173. Liu, Y.; Tan, X.; Liang, J.; Han, H.; Xiang, P.; Yan, W. Machine learning for perovskite solar cells and component materials: key technologies and prospects. *Adv. Funct. Mater.* **2023**, *33*, 2214271. DOI